Enterococcal cell wall remodelling underpins pathogenesis via the release of the Enteroccocal Polysaccharide Antigen (EPA)

Robert E Smith [1*], Rene L Christena [1*], Bartosz J Michno [2], Jessica L Davis [1], Ian DEA Lidbury [1], Marcel Alaman-Zarate [1], Danai Stefanidi [1], Emmanuel Maes [3], Hannah Fisher [1], Tomasz K Prajsnar [2] and Stéphane Mesnage [1]

[1] Molecular Microbiology, School of Biosciences, University of Sheffield, Sheffield, UK

[2] Department of Evolutionary Immunology, Institute of Zoology and Biomedical Research, Faculty of Biology, Jagiellonian University, Kraków, Poland

[3] University of Lille, CNRS, Inserm, CHU Lille, Institut Pasteur de Lille, US 41 - UAR 2014 - PLBS, Lille, France

Running title: *E. faecalis* chain length control

Address correspondence to Stéphane Mesnage, s.mesnage@sheffield.ac.uk

* These authors contributed equally

22 **ABSTRACT**

23 Enterococci are opportunistic pathogens displaying a characteristic ovoid shape, typically forming
24 pairs of cells (diplococci) and short chains. Control of cell chain length in Enterococci is critical
25 during pathogenesis for dissemination in the host and to limit recognition by innate immune
26 effectors such as complement molecules and phagocytes. Here, we identify AtlE, an N-
27 acetylmuramidase responsible for peptidoglycan hydrolysis-mediated septum cleavage during
28 stationary phase. AtlE is encoded by the locus required to produce the decoration subunits of the
29 Enterococcal Polysaccharide Antigen (EPA), which mediate evasion of phagocytosis. We show
30 that peptidoglycan hydrolysis by AtlE is essential for pathogenesis and demonstrate that soluble
31 cell wall fragments containing EPA decorations increase the virulence of *Enterococcus faecalis*,
32 suggesting that EPA plays a role as a decoy molecule to evade host defences. This research sheds
33 light on the complex interplay between bacterial cell division, cell wall remodelling, and the host
34 immune system, providing valuable insights into a novel mechanism underlying the virulence of
35 *E. faecalis.*

36 **INTRODUCTION**

37

38 Peptidoglycan is a bag-shaped macromolecule that represents the major and essential component
39 of the bacterial cell envelope [1, 2]. It confers cell shape and resistance to internal osmotic pressure.
40 In monoderm bacteria, which lack an outer membrane, peptidoglycan serves as a scaffold for the
41 display of proteins and surface polymers [3]. Peptidoglycan is made of glycan chains that consist
42 of *N*-acetylglucosamine and *N*-acetylmuramic acid, crosslinked by short peptide stems [1]. The
43 assembly of this macromolecule is a complex process involving dynamic protein complexes
44 interacting with cytoskeletal elements, achieving both cell elongation and division [4]. During
45 growth and division, peptidoglycan undergoes limited hydrolysis to allow the insertion of novel
46 building blocks and the cleavage of the septum to separate and release daughter cells. The spatio-
47 temporal control of peptidoglycan remodelling by hydrolases is crucial to avoid cell lysis and
48 maintain cell morphology. It involves several co-existing mechanisms, including transcriptional
49 and post-translational control, such as proteolysis or activation via protein-protein interactions (for
50 a recent review, see [5]).
51 In *Enterococcus faecalis,* a peptidoglycan hydrolase called AtlA plays a prominent role in septum
52 cleavage [6]. This enzyme can cause rapid autolysis following carbon source depletion [7] and its
53 activity is therefore tightly controlled via a combination of mechanisms that underpin subcellular
54 targeting and enzymatic activation. AtlA is specifically recruited within the cytoplasm to the
55 septum via its C-terminal domain [8]. This recruitment is facilitated by an unusually long signal
56 peptide (53 residues) similar to extended signal peptide regions (ESPR) [9, 10] shown to slow down
57 translocation across the cytoplasmic membrane [8]. Once exposed at the cell surface, AtlA
58 undergoes proteolytic cleavage by extracellular proteases. This step removes the glycosylated *N*-
59 terminal domain, likely limiting access to the substrate through steric hindrance [11]. Finally, six
60 C-terminal repeats have been proposed to bind preferentially and cooperatively to denuded glycan
61 chains at the septum, ensuring efficient and restricted peptidoglycan hydrolysis [12, 13].
62 The exquisite regulation of AtlA activity is critical to maintain the characteristic morphology of *E.*
63 *faecalis*, which forms mostly diplococci and short chains containing 4 to 8 cells [14]. In the absence
64 of AtlA activity, cells form longer chains which are readily recognised by phagocytes, and the
65 virulence is abolished [11], indicating that minimizing cell chain length is an important process for
66 enterococci.

67 Two other peptidoglycan hydrolases, AtlB and AtlC have also been identified and shown to play a
68 minor role in septum cleavage. A striking observation was that in the absence of AtlA, B and C,
69 the extremely long cell chains formed in exponential phase reverted to form diplococci or short
70 chains during late stationary phase [6]. The enzyme(s) responsible for this phenomenon remained
71 unknown.
72 Here, we identify a peptidoglycan hydrolase (AtlE), that preferentially contributes to daughter cell
73 separation in late stationary phase. AtlE is encoded within the Enterococcal Polysaccharide
74 Antigen (EPA) locus, flanked by the genes responsible for the biosynthesis of EPA decoration
75 subunits, essential for pathogenesis [15]. Whilst the deletion of *atlE* has no impact on EPA structure
76 or its cell surface exposition (as shown by HR-MAS NMR), it completely abolishes virulence in
77 the zebrafish model of infection, suggesting that the digestion of enterococcal cell walls is
78 important for pathogenesis. In agreement with this hypothesis, we show that soluble cell wall
79 fragments containing EPA decorations can play a role as decoy molecules to cause infections and
80 death.

Results

A novel peptidoglycan hydrolytic activity is detected in culture supernatants of the *E. faecalis* Δ*atlABC* mutant

The chains formed by the *E. faecalis* JH2-2 Δ*atlABC* triple mutant in exponential phase [6] revert to diplococci and short chains in stationary phase, indicating that other enzyme(s) cleave the septum during this growth phase. No enzyme candidate for this activity could be identified by zymogram in crude extracts and supernatants from the Δ*atlABC* mutant using the parental cell walls as a substrate. We therefore repeated zymogram experiments using a less crosslinked and more susceptible substrate corresponding to autoclaved cells from a mutant harbouring multiple deletions in class A PBP genes [16] (Fig. 1A). After 48h of incubation in renaturation buffer, a band with peptidoglycan hydrolytic activity was detected in Δ*atlABC* mutant.

To identify the corresponding autolysin, stationary phase culture supernatants were TCA-precipitated, and protein bands detected on a Coomassie-stained SDS-PAGE were individually excised and analysed by LC-MS/MS following in-gel tryptic digestion (Fig. 1B and Table 1). A search against the annotated proteome of the reference *E. faecalis* strain V583 identified three candidates in the band matching the size of the hydrolytic activity on the zymogram: EF0252 and EF0114 (two putative *N*-acetylglucosaminidases) and EF2174 (a putative *N*-acetylmuramidase).

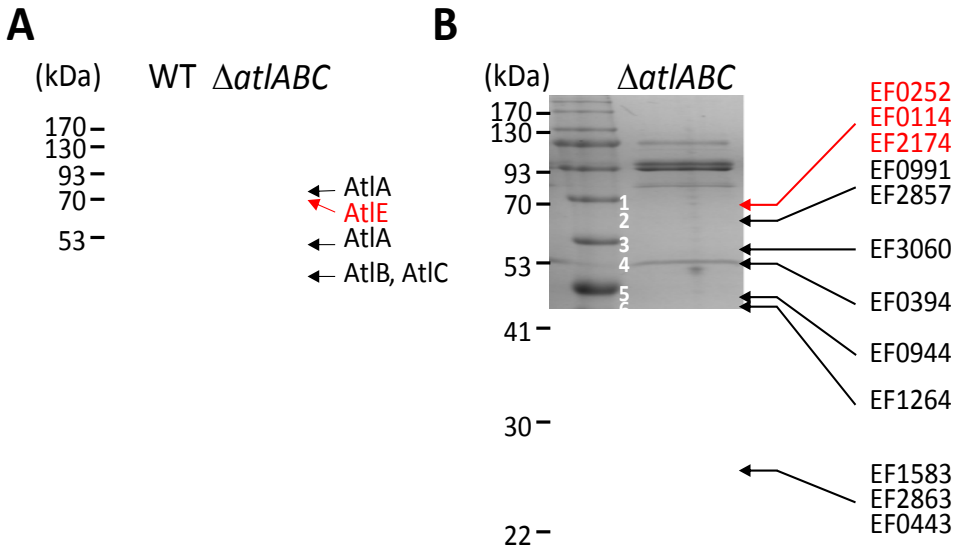

Fig. 1. Identification of a novel peptidoglycan hydrolase activity and secreted proteins in *E. faecalis* JH2-2 culture supernatants. A, Detection of peptidoglycan hydrolytic activities in culture supernatants. 20 µl of culture supernatants from the JH2-2 (WT) and Δ*atlABC* isogenic mutant were loaded on an SDS-PAGE containing autoclaved cells of a mutant with reduced peptidoglycan cross-linking (triple class A PBP mutant Δ*ponA* Δ*pbpF* Δ*pbpZ*). The enzyme with hydrolytic activity present in the triple Δ*atlABC* was named AtlE; the band corresponding to AtlA with a truncated N-terminal domain is indicated with an asterisk. **B**, SDS-PAGE analysis of TCA-precipitated supernatants from the Δ*atlABC* mutant. The proteins corresponding to the seven bands detected were cut and digested with trypsin for LC-MS/MS analysis. The sequence of peptides resulting from trypsin digestions were used to identify *E. faecalis* V583 homologs. Candidates with potential peptidoglycan hydrolytic activity are indicated in red.

Table 1. LC-MS/MS identification of proteins secreted in JH2-2 Δ*atlABC* supernatants.

Band	ID	iBAQ [a]	Unique Peptides	Intensity	Coverage	Size (kDa, aa) [b]	Role	Reference
1	EF0252	6.5 E+08	33	1.0 E+10	78.4	51.9, 477	Peptidoglycan hydrolase (AtlD; GH73)	doi: 10.1159/000486757
	EF2174	3.1 E+08	18	4.7 E+09	46.3	73.1, 676	Putative peptidoglycan hydrolase (GH25)	N/A [c]
	EF0114	4.4 E+07	41	1.7 E+09	47.2	94.0, 835	endo-β-*N*-acetylglucosaminidases (GH18)	doi: 10.1128/JB.00371-21
2	EF0991	1.1 E+09	70	4.7 E+10	84	81.7, 742	Class B Penicillin-binding protein (PBPc)	doi:10.1111/j.1574-
	EF0252	1.0 E+09	26	1.6 E+10	75.7	51.9, 477	Peptidoglycan hydrolase (AtlD; GH73)	doi: 10.1159/000486757
	EF2857	4.7 E+08	55	1.7 E+10	59	711; 77.6	Class B Penicillin-binding protein (PBP2B)	doi:10.1111/j.1574-
3	EF0360	1.1 E+09	53	4.9 E+10	71.2	48.3, 455	Peptidoglycan hydrolase (SagA; Nlp/p60)	doi: 10.7554/eLife.45343
	EF0394	1.0 E+09	34	2.4 E+10	57.4	45.3, 428	Secreted stress-response antigen (SalB)	doi: 10.1128/JB.188.7.2636-
	EF0907	4.7 E+08	29	2.6 E+08	61.9	58.5,534	Hypothetical peptide ABC transporter	N/A
4	EF0394	3.4 E+09	35	4.7 E+10	52.5	45.3, 428	Secreted stress-response antigen (SalB)	doi: 10.1128/JB.188.7.2636-
	EF3060	1.2 E+08	21	2.4 E+09	55.2	48.3,455	Peptidoglycan hydrolase (SagA; Nlp/p60)	doi: 10.7554/eLife.45343
	EF0991	3.1 E+06	18	1.3 E+08	37.7	81.7, 742	Class B Penicillin-binding protein (PBPc)	doi:10.1111/j.1574-
5	EF0944	3.3 E+09	44	5.6 E+10	60.3	40,7, 377	Hypothetical secreted protein	N/A
	EF2860	6.0 E+08	39	1.4 E+10	71.5	53.6, 481	L,D-transpeptidase (Ldt_{fs})	doi.org/10.1074/jbc.M610911200
	EF1264	3.9 E+08	32	1.5 E+10	49.1	80.0, 702	Hypothetical sulfatase	N/A
6	EF1264	1.1 E+09	39	4.3 E+10	51.7	80.0, 702	Hypothetical sulfatase	N/A
	EF0944	5.7 E+08	40	9.7 E+09	58.9	40,7,377	Hypothetical secreted protein	N/A
	EF0394	4.5 E+08	27	6.3 E+09	56.5	45.3,428	Secreted stress-response antigen (SalB)	doi: 10.1128/JB.188.7.2636-
7	EF1583	2.6 E+08	6	2.1 E+09	30,1	27.1, 257	Putative peptidoglycan hydrolase (GH73)	N/A
	EF2863	2.2 E+08	11	2.2 E+09	39,8	30.1, 273	endo-β-*N*-acetylglucosaminidases (GH18)	doi: 10.1111/j.1574-
	EF0443	1.7 E+08	4	1.4 E+09	27,1	18,7, 172	LysM secreted protein	N/A

[a] sum of all the peptides intensities divided by the number of observable peptides of a protein
[b] Size of the mature, secreted protein as predicted by SignalP 5.0 (https://services.healthtech.dtu.dk/service.php?SignalP-5.0)
[c] N/A, not applicable

Identification of the gene encoding AtlE

Genes encoding the three putative peptidoglycan hydrolases identified in Δ*atlABC* mutant supernatants (Fig. 1B) were inactivated by allelic exchange in the Δ*atlABC* background. Whilst no change was observed in the zymogram profiles following the deletion of genes homologous to V583 *EF0252* and *EF0114* (S1 Fig.), no band was detected after the deletion of the *EF2174* homolog (Fig. 2). As expected, complementation of the *atlE* deletion restored the production of a hydrolytic band in the supernatants of the quadruple mutant, and the activity in the complemented strain increased in the presence of a higher concentration of anhydrotetracycline inducer (Fig. 2, lanes 4-6). Hereafter, we name this gene *atlE*.

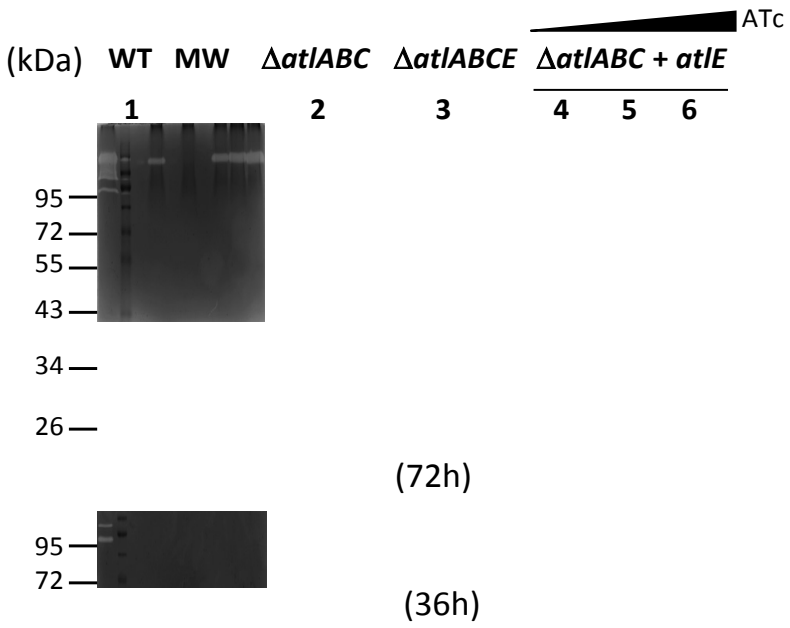

Fig. 2. Zymogram analysis of *E. faecalis* culture supernatants. Peptidoglycan hydrolytic activities were detected in 20 µL of culture supernatants of strains JH2-2 (WT, lane 1), Δ*atlABC* (lane 2), Δ*atlABCE* (lane 3) and Δ*atlABC* + *atlE* (complemented Δ*atlABC* mutant, lanes 4-6). Cells from the triple class A PBP mutant Δ*ponA* Δ*pbpF* Δ*pbpZ* were used as a substrate. The expression of *atlE* was detected in the absence (lane 4) or presence of anhydrotetracycline (Atc) at a concentration of 10 ng/µL (lane 5) or 200 ng/µL (lane 6). The zymogram was repeated with a renaturation time of 36h instead of 72h to see the increased amount of activity associated with *atlE* induction.

AtlE is a cell septum hydrolase involved in maintaining short cell chains

We sought to further investigate the activity of AtlE produced by the pathogenic *E. faecalis* strain OG1RF, since the composition of this bacterium's cell envelope has been more thoroughly characterised than JH2-2. Furthermore, OG1RF is a clinical isolate used to explore pathogenesis in various models of infection [17-19]. OG1RF lacks *atlB* and *atlC* but contains *atlA* and *atlE*.

Zymogram analysis of *altA* and *altE* deletion mutants confirmed the absence of the specific autolytic bands corresponding to their activities and the double mutant Δ*atlAE* did not contain any lytic band. (Fig. S2, lanes 1-4). Complementation of Δ*atlAE* with a plasmid-encoded copy of the *atlE* gene restored the production of the AtlE lytic band (Fig. S2, lane 5).

The role of AtlE in septum cleavage was then investigated using flow cytometry, measuring forward scattered light as a proxy for bacterial cell chain length during both the exponential and stationary phases of growth (Fig. 3) [11]. In exponentially growing cells, *atlA* and *atlE* deletions led to a significant (P=0.0067 and P=0.0164, respectively) increase in cell chain length, even though the

147 effect of the *atlE* deletion was limited. The deletion of *atlE* in the Δ*atlA* background had no significant
148 impact on chain length in exponential phase (Fig. 3A, grey bars). As previously reported, *atlA* deletion
149 led had a less pronounced phenotype in stationary phase, confirming that this autolysin is mostly
150 active in exponential phase (Fig. 3A, pink bars). The deletion of *atlE* alone was associated with a
151 minor but significant increase in chain length in stationary phase. In contrast the combination of *atlA*
152 and *atlE* mutations led to a clear increase in cell chain length in stationary phase. The chain forming
153 phenotype was complemented in the Δ*atlA* Δ*atlE* mutant and increasing *atlE* expression led to a
154 progressive reduction of cell chain chaining (Fig. 3B). Collectively, these data confirmed that AtlE is
155 a peptidoglycan hydrolase responsible for septum cleavage during stationary phase to maintain the
156 characteristic short chains and diplococci.
157

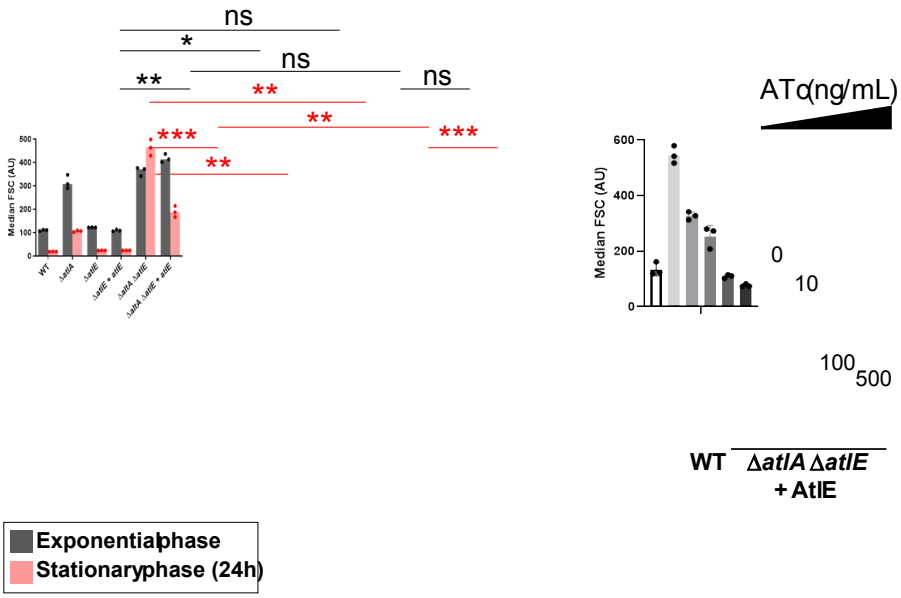

158 **Fig. 3. Contribution of AtlE to septum cleavage and bacterial cell chain length. A**, Comparison of median
159 forward scattered (FSC) light values corresponding to the cell chain lengths of OG1RF (WT), Δ*atlA*, Δ*atlE,*
160 Δ*atlE* + *atlE* (complemented deletion strain), Δ*atlA* Δ*atlE* and *ΔatlA* Δ*atlE* + *atlE* strains in exponentially
161 growing cells and after 24h of growth. Statistical analyses were carried out on results from biological triplicates
162 using *t*-tests with Welch's correction. For exponential cells (grey bars): WT vs Δ*atlA*, **, *P*=0.0067; WT vs
163 Δ*atlE*, *, *P*=0.0164; WT vs Δ*atlE* + *atlE*, ns, *P*=0.7309; Δ*atlA* vs Δ*atlE, ns, P*=0.1025; Δ*atlA* Δ*atlE* vs Δ*atlA*
164 Δ*atlE* + *atlE, ns, P*=0.1249. For stationary cells (24h cultures, pink bars): WT vs Δ*atlA*, ***, *P*=0.0005; WT
165 vs Δ*atlE*, **, *P*=0.0064; WT vs Δ*atlE* + *atlE*, **, *P*=0.0012; Δ*atlA* vs Δ*atlA* Δ*atlE* , **, *P*=0.0036; Δ*atlA* Δ*atlE*
166 vs Δ*atlA* Δ*atlE* + *atlE, ***, P*=0.0005. **B**, AtlE-mediated cleavage of bacterial septum. Median FSC of WT,
167 Δ*atlA* Δ*atlE* mutant and complemented Δ*atlA* Δ*atlE* + *atlE* derivative cells was measured after 16h of growth
168 (overnight cultures). Anhydrotetracycline (Atc) was added at various concentrations (0, 10, 200 and 500
169 ng/mL) to induce the expression of *atlE*.
170

171 ***atlE* is a conserved gene in the EPA decoration locus but shows allelic variation in its C-**
172 **terminal cell wall binding domain**

173 The *atlE* gene is part of the locus encoding EPA decorations (*epa_var*) that varies across
174 *Enterococcus* strains, resulting in the production of strain-specific EPA decoration structures [20,
175 21]. A comparison of the *epa_var* region across *E. faecalis* strains revealed that *atlE* is
176 systematically present in loci with no sequencing gap (Fig. 4A). AtlE is a multidomain protein that
177 always contains an N-terminal glycosyl hydrolase domain belonging to the GH25 family (CAZy
178 database; [22]). GH25 domains are found in enzymes displaying *N*-acetylmuramidase activity like
179 the commercially available mutanolysin (cellosyl). In contrast, the C-terminus is heterogeneous
180 containing a variable number of imperfect repeats corresponding to either GW (pfam13457) or
181 DUF5776 (pfam19087) domains (Fig. 4A and 4B). GW and DUF5776 domains are structurally
182 related to SH3 domains, which are involved in binding to cell envelope polymers. GW repeats have
183 been associated with binding to LTAs [23], but no information is available about DUF5776.
184 Phylogenetic analyses revealed that the N-terminus containing the GH25 domain is partitioned into
185 four subclades (Fig. 4A). Clades I and II possess the GW C-terminal domain and clades III and IV
186 possess the DUF5776 C-terminal domain, suggesting divergence in overall functionality and/or
187 mechanism. Furthermore, the number of C-terminus repeating GW and DUF5776 domains differs
188 between strains (Fig. 4B), as does overall C-terminus protein identity (Fig. 4A, outer ring). For
189 example, OG1RF and V583 are only 47% identical to each other, despite both belonging to clade
190 IV and possessing the DUF5776 domain. Despite sequence variability, Alphafold predicted
191 structures are remarkably conserved (Fig. 4C).

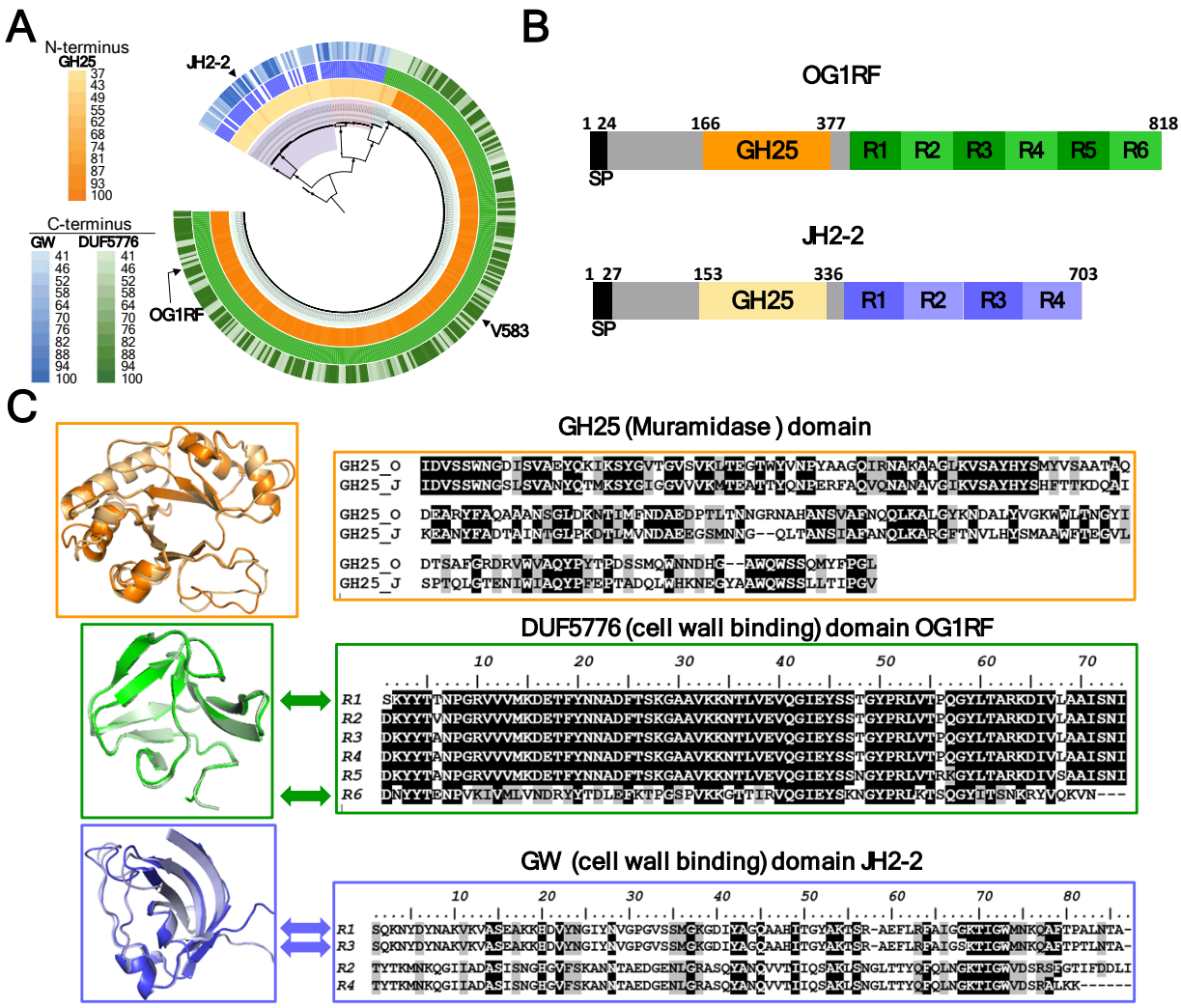

Fig. 4. Distribution and allelic variation of the *E. faecalis atlE* gene. **A**, Phylogenetic reconstruction of AtlE identified in *E. faecalis* genomes. Open reading frames were trimmed to contain only the GH25 domain, totalling 196 sites of which 167 were parsimony informative. Evolutionary distance was inferred using the Maximum Likelihood method using the WAG+G4 best fit model. *E. faecalis* V583 GH25 (N-terminus, inner ring) and DUF5776 (C-terminus, outer ring, green) domains and *E. faecalis* JH2-2 GW (C-terminus, outer ring, blue) domains were used as references for sequence comparisons. **B**, Domain organisation of OG1RF and JH2-2 AtlE alleles. Residues numbers are indicated on the top of the sequence; Individual DUF5776 and GW repeats are numbered from N to C-terminus. SP, signal peptide. **C**, Alphafold structure predictions of GH25, DUF5776 and GW domains from OG1RF and JH2-2. The predicted structures of two DUF5776 and GW domains showing the less similar sequences were aligned (R1 and R6 for OG1RF, R1 and R3 for JH2-2).

AtlE is a muramidase that cleaves peptidoglycan in a strain specific manner

We first sought to characterize the enzymatic activity of OG1RF AtlE (AtlE_O). AtlE_O, devoid of its signal peptide (residues 1-24) was produced recombinantly in *E. coli*, purified, and used to digest OG1RF cell walls (Fig. 5A, insert). The resulting digestion products were analysed by LC-

209 MS and Lc-MS/MS. The muropeptide profile observed was similar to the profile resulting from
210 digestion with mutanolysin [24], and major peaks were assigned to peptidoglycan fragments
211 resulting from glycosyl hydrolase activity (Fig. 5B and Fig. S3). In-source decay (Fig. 5C) and LC-
212 MS/MS analysis (Fig. S3) confirmed that AtlE displays *N*-acetylmuramidase activity, releasing
213 Mur*N*Ac residues at the reducing end of disaccharide-peptides.
214
215

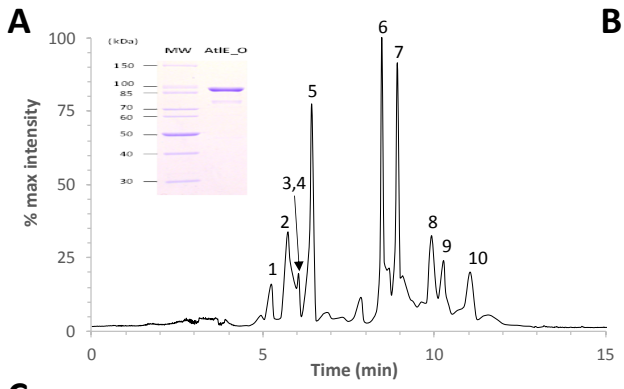

B

Peak	Inferred structure [a]	Monoisotopic mass (Da) [b]		Δppm
		Obs	Theo	
1	gm-AQKA	896.4318	896.4339	-2.3
2	gm-AQK[AA]	967.4704	967.4710	-0.6
3	gm-AQK[AA]A	1038.5080	1038.5081	-0.1
4	gm-AQK[AA]AG	1095.5298	1095.5300	-0.2
5	gm-AQK[AA]AA	1109.5443	1109.5452	-0.8
6	gm-AQK[AA]A=gm-AQK[AA]	1987.9719	1987.9685	1.7
7	gm-AQK[AA]A=gm-AQK[AA]AA	2130.0431	2130.0427	0.2
8	$(gm\text{-}AQK[AA]A)_2$=gm-AQK[AA]	3008.4699	3008.4660	1.3
9	$(gm\text{-}AQK[AA]A)_2$=gm-AQK[AA]AA	3150.5018	3150.5402	-12.2
10	$(gm\text{-}AQK[AA]A)_2$=gm-AQK[AA]AA	4171.0208	4171.0377	-4.1

[a] g, GlcNAc; m, reduced MurNAc; residues in the lateral chain are in square brackets.
[b] Obs, observed; Theo, theoretical.

C

$[M+2H]^{2+}$

$[M+H]^+$
GlcNAc

Loss of GlcNAc
(-203.079)
$[M+H]^+$

216 **Fig. 5. LC-MS characterisation of AtlE enzymatic activity. A**, Total Ion Count chromatogram
217 corresponding to the OG1RF muropeptide solubilised by AtlE_O. Major peaks are numbered. The inset shows
218 an SDS-PAGE of AtlE_O purified by immobilised metal-affinity chromatography. **B**, Identification of major
219 muropeptides shown in A. **C**, Extracted ion chromatogram corresponding to the major monomer (peak 5),
220 showing singly and doubly charged ions matching the expected m/z value for a disaccharide heptapeptide
221 containing a pentapeptide stem and two L-Alanine residues in the lateral chain. The loss of a non-reduced
222 GlcNAc residue shows the *N*-acetylmuramidase activity of the enzyme.
223

224 Unlike the catalytic GH25 domain ubiquitously found at the N-terminus of AtlE, the *C*-terminal
225 cell wall binding domain of this enzyme varies across isolates (Fig. 4A), suggesting that it could
226 specifically recognise strain-specific cell wall components such as EPA decorations. In agreement
227 with this hypothesis, AtlE_O was able to digest cognate OG1RF cell walls, giving a similar profile
228 to mutanolysin (Fig. 6A), but displayed very poor activity (if any) against JH2-2 cell walls
229 (Fig. 6B). No activity was detected against cell walls extracted from the Δ*11720* mutant which no

230 longer produces EPA decorations [20] (Fig. 6C). Collectively, these data indicate that the presence
231 of EPA decorations are required for the activity of AtlE.
232
233

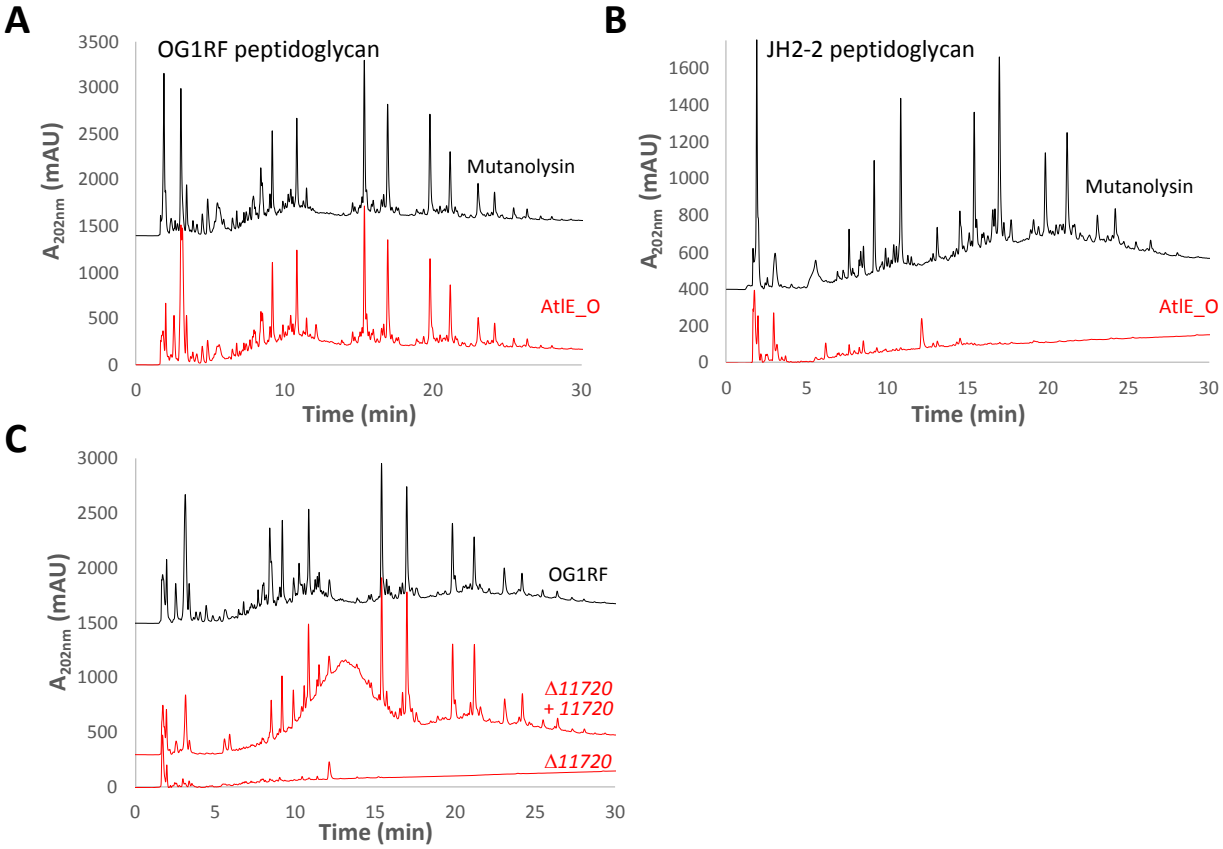

234 **Fig. 6. HPLC analysis of AtlE_O substrate specificity.** The activity of recombinant AtlE_O was
235 tested against several *E. faecalis* cell walls. Muropeptide profiles resulting from the digestion of
236 OG1RF (**A**) or JH2-2 cell walls (**B**) with mutanolysin (black) and AtlE_O (red). **C,** Digestion of
237 cell walls from OG1RF (black) and EPA decoration mutant Δ*11720* and complemented derivative
238 (red).
239
240

241 **AtlE does not contribute to the surface exposure or structure of EPA**

242 EPA decorations are surface exposed and form a pellicle around the cell [25]. We hypothesised
243 that AtlE activity may play a role in the surface exposure of EPA decorations, trimming away the
244 surrounding peptidoglycan. To test this hypothesis, we used high-resolution magic angle spinning
245 (HR-MAS) NMR (Fig. S4A). This technique is performed on whole cells and specifically allows
246 the detection of molecules that are in highly flexible, solvent-exposed environments; molecules
247 with less rotational freedom and/or are not solvent-accessible are not detected. ^{1}H-^{13}C HSQC HR-

248 MAS NMR experiments recorded on *E. faecalis* OG1RF and Δ*atlE* cells showed that AtlE does
249 not contribute to the production or display of surface-exposed EPA or lipoteichoic acid (LTA) [26].
250 Two other unidentified cell wall polysaccharides previously reported [21] (denoted with an asterisk
251 in Fig. S4A) were also detected, and the corresponding signals remained unchanged in the Δ*atlE*
252 mutant. 2D NMR experiments on purified EPA confirmed that the structure of the polysaccharide
253 produced by the mutant was identical to the parental OG1RF (Fig. S4B). Finally, electron
254 micrographs of thin sections revealed the presence of a pellicle at the cell surface of both OG1RF
255 and the Δ*atlE* mutant (Fig. S4C), indicating that no major changes in the cell surface architecture
256 are associated with the deletion of *atlE*.
257

258 **Exploring the role of AtlE activity during pathogenesis in the zebrafish model of infection**

259 The minimization of cell chain length is critical for infection [11]. Whilst AtlE appears to only
260 contribute to cell separation in late stationary phase (Fig 4), we found that the lack of AtlE activity
261 had a significant effect on virulence and dramatically reduced zebrafish embryo lethality upon
262 systemic infection (Fig. 7A). EPA decoration plays a role in innate immune evasion and inhibits
263 uptake by phagocytes [15], but the underpinning mechanism remains unknown. We tested if the
264 release of soluble cell wall fragments by AtlE could contribute to *E. faecalis* virulence.
265 When injected alone, soluble fragments did not have any effect on the zebrafish embryos, but they
266 significantly increased lethality when co-injected with OG1RF cells (Fig. 7B). By contrast, cell
267 wall fragments from the *epaR* strain, which does not produce any EPA decorations [20], had no
268 impact on OG1RF virulence, even when higher doses were injected (Fig. 7C). These results suggest
269 that the release of EPA from the cell wall by AtlE contributes to *E. faecalis* pathogenesis.

270

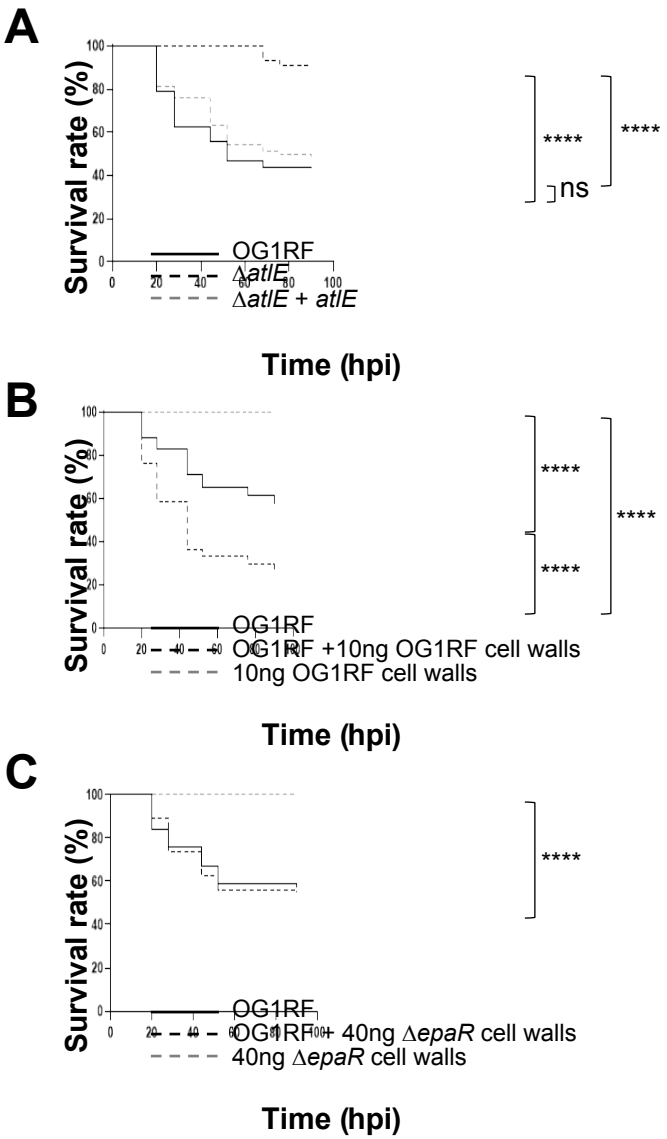

271 **Fig. 7. Contribution of AtlE activity to *E. faecalis* virulence. A**, Survival of zebrafish larvae
272 following injection with *c.a.* 2,000 CFUs of strains OG1RF, Δ*atlE* and complemented derivative
273 (Δ*atlE* +*atlE*). **B**, Injection of OG1RF in the presence of 10 ng of OG1RF soluble cell wall
274 fragments. **C**, Injection of OG1RF in the presence of 40 ng of Δ*epaR* soluble cell wall fragments.
275 Each panel combines three independent experiments (individual repeats are shown in Fig. S5-S7);
276 each survival curve corresponds to the injection of 3 x 25 embryos. ****, $P<0.0001$.

277 **DISCUSSION**

278 Peptidoglycan hydrolases belong to multigene families, and their functional redundancy makes it
279 difficult to identify their specific roles. *E. faecalis* strains encode at least fifteen potential
280 peptidoglycan hydrolases, four of which have been previously characterized (AtlA [7], AtlB [6],
281 AtlC [6] and EnpA [27]). All *E. faecalis* strains encode AtlA, the major peptidoglycan hydrolase
282 responsible for complete daughter cell separation during cell division [7, 11]. Here, we identify
283 AtlE, another peptidoglycan hydrolase which is also ubiquitous across *E. faecalis* strains.
284 Interestingly, the muramidase activity of AtlE appears to have no contribution towards the
285 separation of daughter cells during exponential phase but is essential in the absence of AtlA for
286 cell separation during late stationary phase. This suggests that AtlE activity is cell cycle-dependent,
287 although further work is needed to identify potential temporal regulation mechanisms.
288 Transcriptional regulation has been reported in other bacteria, where sigma factors regulate the
289 expression of peptidoglycan hydrolases in a growth phase-dependent manner [28, 29].
290 Furthermore, AtlA activity is controlled by several post-translational regulations [8, 11] which may
291 also be the case for AtlE.

292 The presence of *atlE* within the EPA decoration biosynthetic locus suggests that AtlE contributes
293 towards the display of EPA at the cell surface or its release after peptidoglycan cleavage. This work
294 revealed a dependency of AtlE enzymatic activity on the presence of strain-specific EPA
295 decoration structures. It is therefore possible that the diversity in the C-terminal sequence and
296 domain organisation of AtlE is driven by the structural diversity of decorations. Interestingly strains
297 V583 and OG1RF produce distinct EPA polysaccharides [20, 21] but encode AtlE alleles with a
298 DUF5776 domain at their C-terminus. This suggests that this family of domains has evolved to
299 recognise different carbohydrate motifs but the binding activity of DUF5776 domains remains to
300 be formally established. HR-MAS NMR and thin-section electron microscopy did not reveal any
301 change in EPA structure, EPA surface exposure or cell envelope ultrastructure following the
302 deletion of *atlE*. Since we previously showed that cell wall material can be released into
303 supernatants during stationary phase [6], we hypothesized that AtlE may be responsible for the
304 release of EPA in culture supernatants and explored whether this may contribute towards *E.*
305 *faecalis* virulence in the zebrafish model of infection. In line with this hypothesis, we found that
306 AtlE is critical for *E. faecalis* virulence and showed that he injection of wild-type enterococci in
307 the presence of soluble cell wall fragments significantly increases the killing of zebrafish embryos.

308 The increase of embryo lethality mediated by soluble cell wall fragments required EPA decoration.
309 Collectively, our results describe a novel virulence mechanism whereby peptidoglycan remodelling
310 mediated by AtlE contributes to the release of EPA fragments as decoy molecules that can inhibit
311 the host immune response. Similar strategies have been described in other pathogens. In *Bordetella*
312 *pertussis*, the release of surface β-1,6-*N*-acetyl-*D*-glucosamine polysaccharides promotes
313 respiratory tract colonization by resisting killing by antimicrobial peptides [30]. Additionally the
314 outer membrane vesicles released by *Acinetobacter baumanii* also contribute to resisting
315 antimicrobial peptides and promote virulence [31], and in *E. coli*, the release of LPS has been
316 proposed to trigger excessive accumulation of systemic ATP, leading to impaired
317 polymorphonuclear leukocyte chemotaxis [32]. The mechanism by which EPA fragments interfere
318 with the immune response awaits further investigation to understand how this complex surface
319 polysaccharide modulates immunity. The discovery of AtlE and the contribution to cell wall
320 remodelling reveals another strategy evolved by *E. faecalis* to thrive in the host.

MATERIALS AND METHODS

Ethics statement

The Jagiellonian University Zebrafish Core Facility (ZCF) is a licensed breeding and research facility (District Veterinary Inspectorate in Krakow registry; Ministry of Science and Higher Education record no. 022 and 0057).

All larval zebrafish experiments were conducted in accordance with the European Community Council Directive 2010/63/EU for the Care and Use of Laboratory Animals of Sept. 22, 2010 (Chapter 1, Article 1 no.3) and Poland's National Journal of Law act of Jan. 15, 2015, for Protection of animals used for scientific or educational purposes (Chapter 1, Article 2 no.1). All experiments with zebrafish were done on larvae up to 5 days post fertilization, which have not yet reached the free feeding stage, and were performed in compliance with ARRIVE guidelines.

Bacterial strains, plasmids, and growth conditions. All strains and plasmids used in this study are described in Table 1. The bacteria were grown at 37°C in Brain Heart Infusion broth or agar (15 g/L) (BHI, Difco laboratories, Detroit, USA). When required, *E. coli* was grown in the presence of 100 µg/mL ampicillin (for protein expression) or 200 µg/mL erythromycin (for pGhost selection). *E. faecalis* transformants were selected with 30 µg/mL erythromycin to select for pGHost9 and pTet derivatives. For complementation experiments, anhydrotetracycline was used at a concentration of 10 ng/µL for precultures and 50 ng/µL unless stated otherwise.

Plasmid construction.

All plasmids and oligonucleotides are described in S1 Table. pGhost derivatives for gene deletion were constructed using the same strategy. Two homology regions flanking the open reading frame encoding each peptidoglycan hydrolase (EF0252, EF0114 and AtlE) were amplified from genomic DNA via PCR. The 5' arm (~0.75 kb) was amplified using the primers H11 (sense) and H12 (antisense), whereas the 3' arm (~0.75 kb) was amplified using H21 (sense) and H22 (antisense). Once purified, the two PCR products were mixed (equimolar amount of each) and fused into a single product (~1.5 kb) via splice overlap extension PCR [33] using primers H11 and H22. The resulting fragment was cut with XhoI and EcoRI and cloned into pGhost9 vector [34] cut with the same enzymes. Candidate pGhost derivatives were screened by PCR using primers pGhost_Fw

352 and pGhost_Rev. A positive clone containing the fused H1-H2 insert corresponding to each
353 construct was checked by Sanger sequencing. pGHH_0252, pGHH_0114, pGHH_atlE_J were used
354 to build mutants in the JH2-2 genetic background; pGHH_atlE_O was used to build an *atlE* mutant
355 in the OG1RF genetic background.
356 pET_AtlE_O was built to express AtlE encoded by OG1RF. The DNA fragment encoding amino
357 acids 25 to 818 was PCR amplified from OG1RF genomic DNA with oligonucleotides
358 atlE_O_pETF and atlE_O_pETR using Phusion DNA polymerase (Fisher Scientific). The resulting
359 fragment was cloned in frame with the hexahistidine sequence of pET2818, a pET2816b derivative
360 [35], using XbaI and BamHI.
361 *atlE* deletion mutants in JH2-2 and OG1RF backgrounds were complemented using pTetH
362 derivatives, allowing anhydrotetracycline inducible expression. DNA fragments encoding the full
363 length AtlE were PCR amplified using atlE_J_Fw and atlE_J_Fw (JH2-2 allele) or atlE_O_Fw and
364 atlE_O_Fw (OG1RF allele). PCR fragments were digested with XbaI and BamHI and cloned into
365 pTetH similarly digested. Positive clones were screened using primers pGhost_Fw and
366 pGhost_Rev. A positive clone containing the *atlE* insert was checked by sanger sequencing and
367 complementation plasmids were named pTet_AtlE_J and pTet_AtlE_O.
368
369 **Construction of *E. faecalis* mutants by allele exchange.** The protocol described previously was
370 followed [6]. *E. faecalis* was electroporated with pGhost9 derivatives and transformants were
371 selected at 30°C in the presence of erythromycin. Single crossing-overs were induced at non
372 permissive temperature (42°C) and screened by PCR. The second recombination event was
373 triggered by subculturing recombinant clones in BHI at 42°C. Erythromycin sensitive colonies
374 were screened by PCR to identify mutants using flanking oligos (H110 and H220).
375
376 **Production and purification of recombinant proteins.** *E. coli* Lemo21(DE3) cells (NEB)
377 transformed with pET_AtlE_O was grown in ZY auto-induction medium [36] containing 100
378 µg/mL of ampicillin and 35 mg/mL of chloramphenicol at 37 °C until the OD_{600} reached 0.5. The
379 cultures were cooled on ice to room temperature and incubated overnight at 20 °C. Cells were
380 harvested by centrifugation, and the frozen pellets were resuspended in lysis buffer (50 mM Tris-
381 HCl pH 8, 300 mM NaCl, 10 mM imidazole). After a 30-minute incubation with 0.1 mg/mL
382 deoxyribonuclease and 0.02M magnesium sulphate at 4°C, the cells were disrupted by sonication

383 on ice. The lysate was clarified by centrifugation, and the supernatant was applied onto a 5mL
384 nickel-chelate affinity prepacked column using an ÄKTA Pure system (Cytiva). The resin was
385 washed with 50 mM Tris-HCl pH 8, 300 mM NaCl, and 5 mM imidazole. The protein was eluted
386 with a gradient to 50 mM Tris-HCl pH 8, 300 mM NaCl, and 500 mM imidazole. The protein was
387 further purified on a Superdex 200 16/60 column (Cytiva) equilibrated with 20 mM Tris-HCl pH
388 7.5, 150 mM NaCl. Fractions containing pure AtlE (>90%), as analyzed by SDS-PAGE, were
389 pooled, concentrated to 2.5 mg/mL, and stored at -80°C in the presence of 25% glycerol until
390 further use.
391

392 **Detection of peptidoglycan hydrolytic activities by zymogram**

393 Proteins were separated by SDS-PAGE using gels containing autoclaved *E. faecalis* JH2-2 Δ*ponA*
394 Δ*pbpZ* Δ*pbpF*, a mutant harbouring a triple deletion of class A PBPs genes. After electrophoresis,
395 proteins were renatured by incubating the gel in 25 mM Tris–HCl (pH 7.5) containing 0.1% Triton
396 at 37 °C. Gels were stained with 1% (w/v) methylene blue in 0.01% (w/v) potassium hydroxide.
397

398 **Cell wall extractions**

399 Overnight static cultures at 37°C were diluted 1:100 into 900 mL of fresh broth (OD_{600} ~0.02) and
400 grown without agitation to an OD_{600} ~1. Cells were harvested by centrifugation (10,000 x *g*, room
401 temperature for 10 min) and resuspended in boiling MilliQ water. SDS was added to a final
402 concentration of 5% (w/v). After 30 min at 100°C, cell walls were recovered by centrifugation
403 (5 min at 15,000 x *g*, room temperature) and washed 5 times with MilliQ water.
404

405 **Muropeptide analysis using rp-HPLC and LC-MS/MS**

406 Cell walls (1 mg) were digested in a final volume of 100 µL for 16h at 37°C in the presence of
407 100U of mutanolysin (SIGMA) or 250 µg of recombinant AtlE in 10 mM phosphate buffer (pH5.5)
408 or 25 mM Tris-HCl (pH7.5), respectively. Soluble cell wall fragments were recovered by
409 centrifugation and reduced by addition of one volume of 200 mM borate buffer (pH 9) and 500 µg
410 of sodium borohydride. The pH was adjusted to 4.5 with phosphoric acid and muropeptides were
411 analysed by rp-HPLC and LC-MS/MS.
412 Rp-HPLC UV traces shown in Fig. 6 were acquired on a Dionex Ultimate 3000 system operated at
413 0.3 mL/min. Samples corresponding to the digestion of 200 µg of cell walls were injected on a

414 Hypersil Gold aQ column (2.1 mm x 200 mm, 1.9 µm particles; Thermo Fisher) using water +
415 0.1% formic acid (v/v) as buffer A and acetonitrile + 0.1% formic acid (v/v) as buffer B. After 1
416 column volume (CV) at 0% B, muropeptides were eluted with a 12 CV gradient to 20% B. The
417 column was washed with 3 CV of 95% B and equilibrated in buffer A.
418 LC-MS/MS analysis was carried out on Ultimate 3000 RSLCnano system (Dionex) coupled to an
419 LTQ-Orbitrap Elite Hybrid mass spectrometer (Thermo Fisher Scientific) equipped with an EASY-
420 Spray ion source. Samples corresponding to 100 ng of cell wall digestion were separated using an
421 EASY-Spray C18 capillary column (150 µm × 150 mm, 2-µm particle size; PN ES806, Thermo
422 Fisher). Muropeptides were eluted using a water-acetonitrile + 0.1% formic acid (v/v) at a flow
423 rate of 1.5 µL/min. The mass spectrometer operated in a standard data-dependent acquisition mode
424 controlled by the Xcalibur v.3.0 and LTQ Tune Plus v.2.7 software. The instrument was operated
425 with a cycle of one MS (in Orbitrap) acquired at a resolution of 60,000 from an *m/z* range of 100–
426 1,600. The top 10 most abundant multiply charged ions (2+ and higher) were subjected to higher-
427 energy collisional dissociation (HCD) fragmentation (normalized collision energy = 30, activation
428 time = 0.1 ms).
429

430 **Genomic analysis**

431 To investigate the occurrence and diversity of AtlE among *E. faecalis*, we downloaded 426
432 genomes deposited in the Joint Genome Institute's Integrated Microbial Genomes (IMG/JGI)
433 database. The conserved N-terminal domain containing GH25 of the model bacterium *E.*
434 *faecalis* V583 was used as a query for BLASTP (stringency e-80). The top hit from each genome
435 was obtained and ORFs were aligned using MUSCLE. Sequences were trimmed to remove amino
436 acids outside the GH25 domain. Phylogenetic reconstruction was performed using IQTree v1.6.8
437 performed using 1000 bootstraps [37]. Tree visualisation and subsequent analysis was performed
438 using the Interactive Tree of Life (ITOL) server [38]. To determine C-terminal identity, BLAST P
439 using either V583 (DUF5776) or JH2-2 (GW) as the queries were performed.
440

441 **LC-MS/MS identification of *E. faecalis* proteins in culture supernatants**

442 *E. faecalis* JH2-2 Δ*atlABC* cells were grown overnight in 50 mL of BHI. Following centrifugation
443 for 10 min at 15,000 x *g*, the supernatant was filtered (0.45 µm pores). Proteins were precipitated
444 by addition of TCA 10% (w/v) final. After 10 min on ice, the sample was spun at 10,000 x *g* for

445 15 min and the supernatant was discarded. Proteins were washed in 20 mL acetone, left to dry
446 under a fume cupboard and resuspended in 250 µL of SDS-PAGE loading buffer.
447 Following Coomassie staining, the gel was washed twice with MilliQ water for 10 min each. The
448 bands of interest were cut out and incubated in 100 µL of a 100 mM ammonium bicarbonate
449 solution for 10 min. The buffer was then removed and replaced by 50 µL of a mixture containing
450 25 mM ammonium bicarbonate (NH_4HCO_3) in acetonitrile (ACN). The procedure was repeated
451 twice until all Coomassie stain was removed and the gel slices were resuspended in 100% ACN
452 for 30 min at 37°C. ACN was then removed and replaced with 50 µL of 10 mM DTT in 100 mM
453 NH_4HCO_3.
454 Reduction was carried out for 45 min at 55°C with agitation, and the buffer was replaced with
455 50 µL of 50 mM of iodoacetamide in 100 mM NH_4HCO_3. Alkylation was carried out in the dark
456 for 30 min at room temperature with agitation, and gel slices were washed with 100 µL of 100 mM
457 NH_4HCO_3 for 5 min at room temperature with agitation followed by 100 µL of 100% ACN for
458 15 min at room temperature with agitation. Gel pieces were air dried for 5-10 minutes and digested
459 in 50 µL of 0.01 mg/mL trypsin solution for 4h at 37°C. Formic acid was added to digestion
460 products at a final concentration of 5% to stop the enzymatic reaction. The solution was transferred
461 to an Eppendorf tube, and peptides were further extracted from the gel by adding 100 µL of 1%
462 (v/v) formic acid and incubating for 15 min at RT with shaking followed by the addition of 100 µL
463 of 100% ACN for 15 min at RT with shaking. This procedure was repeated once, and the combined
464 peptide solutions were dried under vacuum. Peptides were resuspended in 10 µL of 0.1% (v/v)
465 formic acid and cleaned up using a zip-tip (Merck).
466

467 **High-resolution magic angle spinning NMR**

468 Cells were grown in BHI broth overnight and this starter culture was then used to inoculate 100
469 mL of BHI broth at a starting OD_{600} of 0.04 until an OD_{600} reached 0.7 was reached. Cells were
470 then heat-killed at 60 °C for 20 minutes. The suspension was then washed twice in D_2O and freeze-
471 dried. Cells were then re-suspended into 100 µL of D_2O containing 0.01 % (v/v) acetone as an
472 internal standard for chemical shifts (δ ^1H 2.225 and δ ^{13}C 31.55) and centrifuged at 3,000 rpm to
473 be packed into 4-mm ZrO_2 rotor (CortecNet, Paris, France) [39].
474 High-resolution magic angle spinning NMR was performed on *E. faecalis* OG1RF and isogenic
475 mutant Δ*11720* strain using an 18.8T advance NEO spectrometer where ^1H and ^{13}C resonated at

476 800.12 and 200.3 MHz respectively. The set of pulse programs used was extracted from the
477 Bruker® pulse program library where pulses (both hard and soft pulses and their powers) and
478 delays were optimized for each experiment. ^{1}H-^{13}C HSQC spectra were recorded with an inept
479 sequence to distinguish secondary carbons and carbons bearing primary alcohols from other
480 carbons. The 18.8 T was equipped with a 4mm D/^{1}H/^{13}C/^{31}P HR-MAS probe head where the rotor
481 was spun at 8000Hz during acquisition to eliminate anisotropy effect of jelly state of bacterial cells.
482 All spectra were recorded at 300 K, and the rotor spinning rate was 8 kHz. For ^{1}H-^{13}C HSQC
483 experiments, the spectral widths were 12,820 Hz (^{1}H) with 1,024 points for the FID resolution and
484 29,994 Hz (^{13}C) with 400 points for FID resolution during 400 scans, giving 12.5 Hz/pt and 75.0
485 Hz/pt, respectively.
486

487 **Flow cytometry**

488 Overnight static cultures at 37°C were diluted 1:100 into fresh broth (OD_{600}~0.02) and grown to
489 mid-exponential phase (OD600~0.2 to 0.4). Bacteria were diluted 1:100 in filtered phosphate
490 buffer saline and analyzed by flow cytometry using a Millipore Guava easyCyte H2L system and
491 the GuavaSoft v3.1.1 software. Light scatter data were obtained with logarithmic amplifiers for
492 20,000 events.
493

494 **Chemical fixation, thin sectioning, and electron microscopy of *E. faecalis* cells**

495 Cell pellets were fixed in 3 % (w/v) glutaraldehyde at 4 °C overnight. Samples were washed in
496 0.1 M sodium cacodylate buffer and incubated for 2 h at room temperature in 1 % (w/v) osmium
497 tetroxide for secondary fixation. Cell pellets were washed with 0.1 M sodium cacodylate buffer
498 and dehydrated by incubating with increasing concentrations of ethanol (50 % (v/v), 75 % (v/v),
499 95 % (v/v), 100 % (v/v) ethanol) for 15 min each. Ethanol was removed and samples were
500 incubated with propylene oxide for complete dehydration. Samples were incubated overnight at
501 room temperature in a 1:1 mix of propylene oxide and Araldite resin (Agar Scientific, CY212) to
502 allow for infiltration. Resin was removed and excess propylene oxide evaporated at room
503 temperature. Samples were placed in two consecutives 4 h incubations in pure Araldite resin before
504 being embedded into the final fresh resin. Resin was polymerised by incubation at 60 °C for 48 h.
505 Thin sections (90 nm) were produced using an Ultracut E Ultramicrotome (Reichert-Jung) and
506 floated onto 300-square mesh nickel TEM grids. Sections were stained in 3 % (w/v) uranyl acetate

507 for 30 min, washed with dH_2O, stained with Reynold's lead citrate for 5 min and further washed
508 with dH_2O. Sections were imaged on a FEI Tecnai T12 Spirit Transmission Electron Microscope
509 operated at 80 kV and equipped with a Gatan Orius SC1000B CCD camera.
510

511 **Zebrafish experiments**

512 Zebrafish embryos were obtained by the natural spawning of adult zebrafish (line AB/TL), which
513 were housed in a continuous recirculating closed-system aquarium with a light/dark cycle of 14/10
514 h at 28 °C. Dechorionated embryos at 30 hpf were systemically injected with ca. 2,000 *E. faecalis*
515 cells as previously described [20]. In some experiments, the bacterial inoculum was supplemented
516 with soluble cell wall fragments dissolved in MilliQ water. The number of injected cells was
517 checked before and after each series of injections with a given strain. The infected embryos were
518 monitored at regular intervals until 90 h post infection (hpi). 25 embryos per group were used in
519 each experiment.
520

521 **Statistical analyses**

522 Statistical analyses were performed using GraphPad Prism. Survival experiments were evaluated
523 using the Kaplan-Meier method. Comparisons between curves were made using the Log Rank
524 (Mantel-Cox) test. For flow cytometry experiments, forward scattered light values were compared
525 using an unpaired *t*-test with Welch's correction.
526

527 **Data availability**

528 LC-MS/MS data related to Fig. 5 and S3 Fig. is available through the Glycopost repository
529 (GPST000505; http://doi.org/10.50821/GLYCOPOST-GPST000505). All material including
530 NMR data will be made available upon request to S. Mesnage.
531

532 **Supporting information**

533

534 **S1 Fig. Zymogram analysis of *E. faecalis* JH2-2 culture supernatants.** Peptidoglycan hydrolytic
535 activities were detected in 20 µL of culture supernatants of strains JH2-2 (WT), Δ*atlABC,* Δ*atlABC*
536 Δ*0252* and Δ*atlABC* Δ*0252.* Cells from the triple class A PBP mutant Δ*ponA* Δ*pbpF* Δ*pbpZ* were
537 used as a substrate.

538
539 **S2 Fig. Zymogram analysis of *E. faecalis* OG1RF culture supernatants.** Peptidoglycan
540 hydrolytic activities were detected in 25 µL of culture supernatants of strains OG1RF (WT, lane
541 1), Δ*atlE (lane 2),* Δ*atlA* (lane 3), Δ*atlA* Δ*atlE* (lane 4), and complemented Δ*atlA* Δ*atlE* mutant
542 (Δ*atlE* + *atlE*, lane 5). Cells from the triple class A PBP mutant Δ*ponA* Δ*pbpF* Δ*pbpZ* were used
543 as a substrate.

544
545 **S3 Fig. MS/MS analysis of peak 5. A**, fragmentation of the doubly charged Ion $(M+2H]^{2+}$;
546 *m/z*=555.78). Ions with *m/z* values matching predicted fragments are boxed in red. **B**, List of
547 predicted fragments, theoretical and observed *m/z*. ND, not detected; g, GlcNAc; m(r), reduced
548 MurNAc; residues in square bracket correspond to the lateral chain.

549
550 **S4 Fig. AtlE is not involved in EPA biosynthesis or exposure at the cell surface. A**, ^{1}H-^{13}C
551 HSQC spectra of purified wild type and Δ*atlE* EPA. The region displayed corresponding to the
552 anomeric protons (4.3-5.5 ppm) and anomeric carbons (90-110 ppm) of WT (left) and *ΔatlE* (right)
553 did not reveal any major difference between the 2 EPA polymers. **B**, ^{1}H-^{13}C HSQC HR-MAS NMR
554 experiments recorded on *E. faecalis* OG1RF (left) and Δ*atlE* (right) cells show that AtlE does not
555 contribute towards the production or display of surface exposed EPA or lipoteichoic acid (LTA)
556 [26]. Two other currently unidentified cell wall polysaccharides denoted with an asterisk are also
557 detected [21]. **C**, Thin section transmission electron microscopy of *E. faecalis* OG1RF (left) and
558 Δ*atlE* (right) cells confirm EPA decorations remain surface exposed in the Δ*atlE* mutant, both
559 forming a pellicle at their cell surface (arrows).

560
561 **S5 Fig. Survival ratio of zebrafish larvae infected with *E. faecalis* OG1RF, Δ*atlE* and Δ*atlE***
562 **complemented strains.** Larvae were infected with *ca.* 2000 CFUs of parental (WT) OG1RF strain
563 (solid line), Δ*atlE* (black dashed line) or Δ*atlE* + *atlE* (grey dashed line). Survival was monitored
564 between 20 to 90 hours post infection (hpi) at 28°C using 25 larvae per strain per experiment. Three
565 independent experiments (**A**, **B** and **C**) and combined results (**D**) are shown. (**E**) *P* values of
566 pairwise comparison.

567
568 **S6 Fig. Survival ratio of zebrafish larvae infected with *E. faecalis* OG1RF in the presence or**
569 **absence of OG1RF soluble cell wall fragments**. Larvae were infected with *ca.* 2000 CFUs of
570 parental (WT) OG1RF strain in the absence (solid line) or presence (black dashed line) of 10ng of
571 soluble cell walls. A control injection corresponding to 10ng of OG1RF cell walls alone is shown

572 (grey dashed line). Survival was monitored between 20 to 90 hours post infection (hpi) at 28°C
573 using 25 larvae per strain per experiment. Three independent experiments (**A**, **B** and **C**) and
574 combined results (**D**) are shown. (**E**) *P* values of pairwise comparison.

575
576 **S7 Fig. Survival ratio of zebrafish larvae infected with *E. faecalis* OG1RF in the presence or**
577 **absence of *epaR* soluble cell wall fragments lacking EPA decorations.** Larvae were infected
578 with *ca.* 2000 CFUs of parental (WT) OG1RF strain in the absence (solid line) or presence (black
579 dashed line) of 40ng of soluble cell walls. A control injection corresponding to 40ng of OG1RF
580 cell walls alone is shown (grey dashed line). Survival was monitored between 20 to 90 hours post
581 infection (hpi) at 28°C using 25 larvae per strain per experiment. Three independent experiments
582 (**A**, **B** and **C**) and combined results (**D**) are shown. (**E**) *P* values of pairwise comparison.

583
584 **S1 Table. strains, plasmids, oligonucleotides**

585

586 **ACKNOWLEDGMENTS**

587 The authors would like to thank Michel Arthur for the JH2-2 triple *pbp* mutant, Adelina Acosta-
588 Martin for her help with LC-MS/MS experiments and Finn O'Dea for the preparation of NMR
589 figures. RLC was the recipient of a Commonwealth Rutherford fellowship (INRF-2017-163).
590 MGAZ was supported by a Conahcyt studentship from the Mexican government (2021-000007-
591 01EXTF-00221). JLD, RES and HF were funded by the White Rose Doctoral Training Programme
592 (BBSRC grant BB/ M011151/1). HR-MAS experiments were carried out at the NMR facility of
593 the Advanced Characterization Platform of the Chevreul Institute (Villeneuve d'Ascq-France) by
594 the staff of the PAGés platform. BJM and TKP were supported by National Science Centre of
595 Poland within Sonata Bis 9 project (Grant number UMO-2019/34/E/NZ6/00137).

596 **REFERENCES**

597

598 1. Vollmer W, Blanot D, de Pedro MA. Peptidoglycan structure and architecture. FEMS Microbiol Rev.
599 2008;32(2):149-67. PubMed PMID: 18194336.
600 2. Weidel W, Pelzer H. Bagshaped macromolecules - a new outlook on bacterial cell walls. Adv Enzymol Relat
601 Areas Mol Biol. 1964;26:193-232. PubMed PMID: 14150645.
602 3. Schaffer C, Messner P. The structure of secondary cell wall polymers: how Gram-positive bacteria stick their
603 cell walls together. Microbiology (Reading). 2005;151(Pt 3):643-51. Epub 2005/03/11. doi:
604 10.1099/mic.0.27749-0. PubMed PMID: 15758211.
605 4. Egan AJF, Errington J, Vollmer W. Regulation of peptidoglycan synthesis and remodelling. Nat Rev Microbiol.
606 2020;18(8):446-60. Epub 2020/05/20. doi: 10.1038/s41579-020-0366-3. PubMed PMID: 32424210.
607 5. Brogan AP, Rudner DZ. Regulation of peptidoglycan hydrolases: localization, abundance, and activity. Curr
608 Opin Microbiol. 2023;72:102279. Epub 2023/02/23. doi: 10.1016/j.mib.2023.102279. PubMed PMID:
609 36812681; PubMed Central PMCID: PMCPMC10031507.
610 6. Mesnage S, Chau F, Dubost L, Arthur M. Role of *N*-acetylglucosaminidase and *N*-acetylmuramidase activities
611 in *Enterococcus faecalis* peptidoglycan metabolism. The Journal of biological chemistry. 2008;283(28):19845-
612 53. Epub 2008/05/21. doi: M802323200 [pii]
613 10.1074/jbc.M802323200. PubMed PMID: 18490448.
614 7. Qin X, Singh KV, Xu Y, Weinstock GM, Murray BE. Effect of disruption of a gene encoding an autolysin of
615 *Enterococcus faecalis* OG1RF. Antimicrob Agents Chemother. 1998;42(11):2883-8. PubMed PMID: 9797220.
616 8. Salamaga B, Turner RD, Elsarmane F, Galley NF, Kulakauskas S, Mesnage S. A moonlighting role for LysM
617 peptidoglycan binding domains underpins Enterococcus faecalis daughter cell separation. Commun Biol.
618 2023;6(1):428. Epub 2023/04/19. doi: 10.1038/s42003-023-04808-z. PubMed PMID: 37072531; PubMed
619 Central PMCID: PMCPMC10113225.
620 9. Desvaux M, Scott-Tucker A, Turner SM, Cooper LM, Huber D, Nataro JP, et al. A conserved extended signal
621 peptide region directs posttranslational protein translocation via a novel mechanism. Microbiology (Reading).
622 2007;153(Pt 1):59-70. Epub 2006/12/23. doi: 10.1099/mic.0.29091-0. PubMed PMID: 17185535.
623 10. Leyton DL, de Luna M, Sevastsyanovich YR, Tveen Jensen K, Browning DF, Scott-Tucker A, et al. The
624 unusual extended signal peptide region is not required for secretion and function of an Escherichia coli
625 autotransporter. FEMS Microbiol Lett. 2010;311(2):133-9. Epub 2010/08/26. doi: 10.1111/j.1574-
626 6968.2010.02081.x. PubMed PMID: 20735484.
627 11. Salamaga B, Prajsnar TK, Jareno-Martinez A, Willemse J, Bewley MA, Chau F, et al. Bacterial size matters:
628 Multiple mechanisms controlling septum cleavage and diplococcus formation are critical for the virulence of the
629 opportunistic pathogen *Enterococcus faecalis*. PLoS Pathog. 2017;13(7):e1006526. Epub 2017/07/26. doi:
630 10.1371/journal.ppat.1006526. PubMed PMID: 28742152; PubMed Central PMCID: PMCPMC5542707.
631 12. Mesnage S, Dellarole M, Baxter NJ, Rouget JB, Dimitrov JD, Wang N, et al. Molecular basis for bacterial
632 peptidoglycan recognition by LysM domains. Nat Commun. 2014;5:4269. Epub 2014/07/01. doi:
633 10.1038/ncomms5269. PubMed PMID: 24978025; PubMed Central PMCID: PMCPMC4083421.
634 13. Yahashiri A, Jorgenson MA, Weiss DS. Bacterial SPOR domains are recruited to septal peptidoglycan by
635 binding to glycan strands that lack stem peptides. Proc Natl Acad Sci U S A. 2015;112(36):11347-52. Epub
636 2015/08/26. doi: 10.1073/pnas.1508536112. PubMed PMID: 26305949; PubMed Central PMCID:
637 PMCPMC4568695.
638 14. Thiercelin ME. Sur un diplococque saprophyte de l'intestin susceptible de devenir pathogène. CR Soc Biol.
639 1899;5:269-71.
640 15. Smith RE, Salamaga B, Szkuta P, Hajdamowicz N, Prajsnar TK, Bulmer GS, et al. Decoration of the
641 enterococcal polysaccharide antigen EPA is essential for virulence, cell surface charge and interaction with
642 effectors of the innate immune system. PLoS Pathog. 2019;15(5):e1007730. Epub 2019/05/03. doi:
643 10.1371/journal.ppat.1007730. PubMed PMID: 31048927; PubMed Central PMCID: PMCPMC6497286.
644 16. Arbeloa A, Segal H, Hugonnet JE, Josseaume N, Dubost L, Brouard JP, et al. Role of class A penicillin-binding
645 proteins in PBP5-mediated beta-lactam resistance in *Enterococcus faecalis*. J Bacteriol. 2004;186(5):1221-8.
646 PubMed PMID: 14973044.

17. Peng Z, Ehrmann MA, Waldhuber A, Niemeyer C, Miethke T, Frick JS, et al. Phosphotransferase systems in Enterococcus faecalis OG1RF enhance anti-stress capacity in vitro and in vivo. Research in microbiology. 2017;168(6):558-66. Epub 2017/04/04. doi: 10.1016/j.resmic.2017.03.003. PubMed PMID: 28365379.
18. Prajsnar TK, Renshaw SA, Ogryzko NV, Foster SJ, Serror P, Mesnage S. Zebrafish as a novel vertebrate model to dissect enterococcal pathogenesis. Infect Immun. 2013;81(11):4271-9. Epub 2013/09/05. doi: 10.1128/IAI.00976-13. PubMed PMID: 24002065; PubMed Central PMCID: PMCPMC3811811.
19. Singh KV, Qin X, Weinstock GM, Murray BE. Generation and testing of mutants of Enterococcus faecalis in a mouse peritonitis model. J Infect Dis. 1998;178(5):1416-20. Epub 1998/10/21. doi: 10.1086/314453. PubMed PMID: 9780263.
20. Davis JL, Norwood JS, Smith RE, O'Dea F, Chellappa K, Rowe ML, et al. Dissecting the Enterococcal Polysaccharide Antigen (EPA) structure to explore innate immune evasion and phage specificity. Carbohydr Polym. 2025;347:122686. Epub 2024/11/02 23:12. doi: 10.1016/j.carbpol.2024.122686. PubMed PMID: 39486929.
21. Guerardel Y, Sadovskaya I, Maes E, Furlan S, Chapot-Chartier MP, Mesnage S, et al. Complete Structure of the Enterococcal Polysaccharide Antigen (EPA) of Vancomycin-Resistant Enterococcus faecalis V583 Reveals that EPA Decorations Are Teichoic Acids Covalently Linked to a Rhamnopolysaccharide Backbone. mBio. 2020;11(2). Epub 2020/04/30. doi: 10.1128/mBio.00277-20. PubMed PMID: 32345640; PubMed Central PMCID: PMCPMC7188991.
22. Drula E, Garron ML, Dogan S, Lombard V, Henrissat B, Terrapon N. The carbohydrate-active enzyme database: functions and literature. Nucleic Acids Res. 2022;50(D1):D571-D7. Epub 2021/12/02. doi: 10.1093/nar/gkab1045. PubMed PMID: 34850161; PubMed Central PMCID: PMCPMC8728194.
23. Zoll S, Patzold B, Schlag M, Gotz F, Kalbacher H, Stehle T. Structural basis of cell wall cleavage by a staphylococcal autolysin. PLoS Pathog. 2010;6(3):e1000807. Epub 2010/03/20. doi: 10.1371/journal.ppat.1000807. PubMed PMID: 20300605; PubMed Central PMCID: PMC2837410.
24. Emirian A, Fromentin S, Eckert C, Chau F, Dubost L, Delepierre M, et al. Impact of peptidoglycan *O*-acetylation on autolytic activities of the *Enterococcus faecalis N*-acetylglucosaminidase AtlA and *N*-acetylmuramidase AtlB. FEBS Lett. 2009. Epub 2009/08/19. doi: S0014-5793(09)00629-2 [pii] 10.1016/j.febslet.2009.08.010. PubMed PMID: 19686739.
25. Furlan S, Matos RC, Kennedy SP, Doublet B, Serror P, Rigottier-Gois L. Fitness Restoration of a Genetically Tractable Enterococcus faecalis V583 Derivative To Study Decoration-Related Phenotypes of the Enterococcal Polysaccharide Antigen. mSphere. 2019;4(4). Epub 2019/07/12. doi: 10.1128/mSphere.00310-19. PubMed PMID: 31292230; PubMed Central PMCID: PMCPMC6620374.
26. Fabretti F, Theilacker C, Baldassarri L, Kaczynski Z, Kropec A, Holst O, et al. Alanine esters of enterococcal lipoteichoic acid play a role in biofilm formation and resistance to antimicrobial peptides. Infect Immun. 2006;74(7):4164-71. Epub 2006/06/23. doi: 10.1128/IAI.00111-06. PubMed PMID: 16790791; PubMed Central PMCID: PMCPMC1489678.
27. de Roca FR, Duche C, Dong S, Rince A, Dubost L, Pritchard DG, et al. Cleavage specificity of Enterococcus faecalis EnpA (EF1473), a peptidoglycan endopeptidase related to the LytM/lysostaphin family of metallopeptidases. Journal of molecular biology. 2010;398(4):507-17. Epub 2010/03/30. doi: 10.1016/j.jmb.2010.03.033. PubMed PMID: 20347848.
28. Li R, Chu R, Ban R. The characteristics of autolysins associated with cell separation in Bacillus subtilis. J Bacteriol. 2024;206(8):e0013324. Epub 2024/07/16. doi: 10.1128/jb.00133-24. PubMed PMID: 39012109; PubMed Central PMCID: PMCPMC11340307.
29. Salzberg LI, Powell L, Hokamp K, Botella E, Noone D, Devine KM. The WalRK (YycFG) and sigma(I) RsgI regulators cooperate to control CwlO and LytE expression in exponentially growing and stressed Bacillus subtilis cells. Mol Microbiol. 2013;87(1):180-95. Epub 2012/12/04. doi: 10.1111/mmi.12092. PubMed PMID: 23199363.
30. Fullen AR, Gutierrez-Ferman JL, Yount KS, Love CF, Choi HG, Vargas MA, et al. Bps polysaccharide of Bordetella pertussis resists antimicrobial peptides by functioning as a dual surface shield and decoy and converts Escherichia coli into a respiratory pathogen. PLoS Pathog. 2022;18(8):e1010764. Epub 2022/08/16. doi: 10.1371/journal.ppat.1010764. PubMed PMID: 35969621; PubMed Central PMCID: PMCPMC9410548.
31. Park J, Kim M, Shin B, Kang M, Yang J, Lee TK, et al. A novel decoy strategy for polymyxin resistance in Acinetobacter baumannii. eLife. 2021;10. Epub 2021/06/29. doi: 10.7554/eLife.66988. PubMed PMID: 34180396; PubMed Central PMCID: PMCPMC8324293.

701 32. Kondo Y, Ledderose C, Slubowski CJ, Fakhari M, Sumi Y, Sueyoshi K, et al. Frontline Science: Escherichia
702 coli use LPS as decoy to impair neutrophil chemotaxis and defeat antimicrobial host defense. J Leukoc Biol.
703 2019;106(6):1211-9. Epub 2019/08/09. doi: 10.1002/JLB.4HI0319-109R. PubMed PMID: 31392789; PubMed
704 Central PMCID: PMCPMC6883117.
705 33. Ho SN, Hunt HD, Horton RM, Pullen JK, Pease LR. Site-directed mutagenesis by overlap extension using the
706 polymerase chain reaction. Gene. 1989;77(1):51-9. PubMed PMID: 2744487.
707 34. Maguin E, Duwat P, Hege T, Ehrlich D, Gruss A. New thermosensitive plasmid for gram-positive bacteria. J
708 Bacteriol. 1992;174(17):5633-8. Epub 1992/09/01. doi: 10.1128/jb.174.17.5633-5638.1992. PubMed PMID:
709 1324906; PubMed Central PMCID: PMCPMC206509.
710 35. Eckert C, Lecerf M, Dubost L, Arthur M, Mesnage S. Functional analysis of AtlA, the major *N*-
711 acetylglucosaminidase of *Enterococcus faecalis*. J Bacteriol. 2006;188(24):8513-9. PubMed PMID: 17041059.
712 36. Grabski A, Mehler M, Drott D. The overnight express autoinduction system: high-density cell growth and
713 protein expression while you sleep. Nature methods. 2005;2:233-5.
714 37. Minh BQ, Schmidt HA, Chernomor O, Schrempf D, Woodhams MD, von Haeseler A, et al. IQ-TREE 2: New
715 Models and Efficient Methods for Phylogenetic Inference in the Genomic Era. Mol Biol Evol. 2020;37(5):1530-
716 4. Epub 2020/02/06. doi: 10.1093/molbev/msaa015. PubMed PMID: 32011700; PubMed Central PMCID:
717 PMCPMC7182206.
718 38. Letunic I, Bork P. Interactive Tree Of Life (iTOL) v4: recent updates and new developments. Nucleic Acids
719 Res. 2019;47(W1):W256-W9. Epub 2019/04/02. doi: 10.1093/nar/gkz239. PubMed PMID: 30931475; PubMed
720 Central PMCID: PMCPMC6602468.
721 39. Sadovskaya I, Guerardel Y. Simple Protocol to Purify Cell Wall Polysaccharide from Gram-Positive Bacteria
722 and Assess Its Structural Integrity. Methods Mol Biol. 2019;1954:37-45. Epub 2019/03/14. doi: 10.1007/978-1-
723 4939-9154-9_4. PubMed PMID: 30864122.
724

Table 1. LC-MS/MS identification of proteins secreted in JH2-2 Δ*atlABC* supernatants.
[a] sum of all the peptides intensities divided by the number of observable peptides of a protein

Band	ID	iBAQ [a]	Unique Peptides	Intensity	Coverage	Size (kDa, aa) [b]	Role	Reference
1	EF0252	6.5 E+08	33	1.0 E+10	78.4	51.9, 477	Peptidoglycan hydrolase (AtlD; GH73)	doi: 10.1159/000486757
	EF2174	3.1 E+08	18	4.7 E+09	46.3	73.1, 676	Putative peptidoglycan hydrolase (GH25)	N/A [c]
	EF0114	4.4 E+07	41	1.7 E+09	47.2	94.0, 835	endo-β-*N*-acetylglucosaminidases (GH18)	doi: 10.1128/JB.00371-21
2	EF0991	1.1 E+09	70	4.7 E+10	84	81.7, 742	Class B Penicillin-binding protein (PBPc)	doi:10.1111/j.1574-
	EF0252	1.0 E+09	26	1.6 E+10	75.7	51.9, 477	Peptidoglycan hydrolase (AtlD; GH73)	doi: 10.1159/000486757
	EF2857	4.7 E+08	55	1.7 E+10	59	711; 77.6	Class B Penicillin-binding protein (PBP2B)	doi:10.1111/j.1574-
3	EF0360	1.1 E+09	53	4.9 E+10	71.2	48.3, 455	Peptidoglycan hydrolase (SagA; Nlp/p60)	doi: 10.7554/eLife.45343
	EF0394	1.0 E+09	34	2.4 E+10	57.4	45.3, 428	Secreted stress-response antigen (SalB)	doi: 10.1128/JB.188.7.2636-
	EF0907	4.7 E+08	29	2.6 E+08	61.9	58.5,534	Hypothetical peptide ABC transporter	N/A
4	EF0394	3.4 E+09	35	4.7 E+10	52.5	45.3, 428	Secreted stress-response antigen (SalB)	doi: 10.1128/JB.188.7.2636-
	EF3060	1.2 E+08	21	2.4 E+09	55.2	48.3,455	Peptidoglycan hydrolase (SagA; Nlp/p60)	doi: 10.7554/eLife.45343
	EF0991	3.1 E+06	18	1.3 E+08	37.7	81.7, 742	Class B Penicillin-binding protein (PBPc)	doi:10.1111/j.1574-
5	EF0944	3.3 E+09	44	5.6 E+10	60.3	40,7, 377	Hypothetical secreted protein	N/A
	EF2860	6.0 E+08	39	1.4 E+10	71.5	53.6, 481	L,D-transpeptidase (Ldt_{fs})	doi.org/10.1074/jbc.M610911200
	EF1264	3.9 E+08	32	1.5 E+10	49.1	80.0, 702	Hypothetical sulfatase	N/A
6	EF1264	1.1 E+09	39	4.3 E+10	51.7	80.0, 702	Hypothetical sulfatase	N/A
	EF0944	5.7 E+08	40	9.7 E+09	58.9	40,7,377	Hypothetical secreted protein	N/A
	EF0394	4.5 E+08	27	6.3 E+09	56.5	45.3,428	Secreted stress-response antigen (SalB)	doi: 10.1128/JB.188.7.2636-
7	EF1583	2.6 E+08	6	2.1 E+09	30,1	27.1, 257	Putative peptidoglycan hydrolase (GH73)	N/A
	EF2863	2.2 E+08	11	2.2 E+09	39,8	30.1, 273	endo-β-*N*-acetylglucosaminidases (GH18)	doi: 10.1111/j.1574-
	EF0443	1.7 E+08	4	1.4 E+09	27,1	18,7, 172	LysM secreted protein	N/A

[b] Size of the mature, secreted protein as predicted by SignalP 5.0 (https://services.healthtech.dtu.dk/service.php?SignalP-5.0)
[c] N/A, not applicable

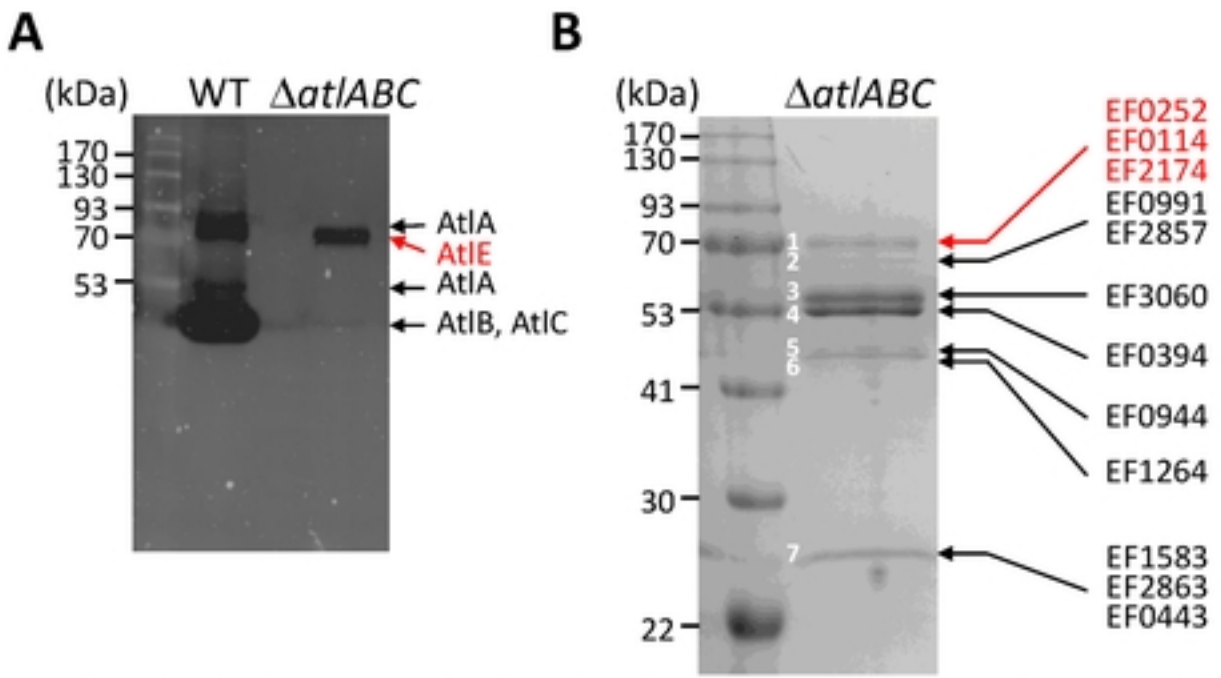

Fig. 1. Identification of a novel peptidoglycan hydrolase activity and secreted proteins in E. faecalis JH2-2 culture supernatants. A. Detection of peptidoglycan hydrolytic activities in culture supernatants. Twenty µl of culture supernatants of the JH2-2 (WT) and ΔABC isogenic mutant were loaded on an SDS-PAGE containing autoclaved cells of a mutant with reduced peptidoglycan cross-linking (triple class A PBP mutant ΔponA ΔpbpF ΔpbpZ). The enzyme with hydrolytic activity present in the triple ΔABC was named AtlE. **B.** SDS-PAGE analysis of TCA-precipitated supernatants from the ΔABC mutant. The proteins corresponding to the seven bands detected were cut and digested with trypsin for LC-MS/MS analysis. The sequence of peptides resulting from tryptin digestions were used to identify E. faecalis V583 homologs. Candidates with potential peptidoglycan hydrolytic activity are indicated in red.

Figure 1 (AtlE detection and LC-MS/MS)

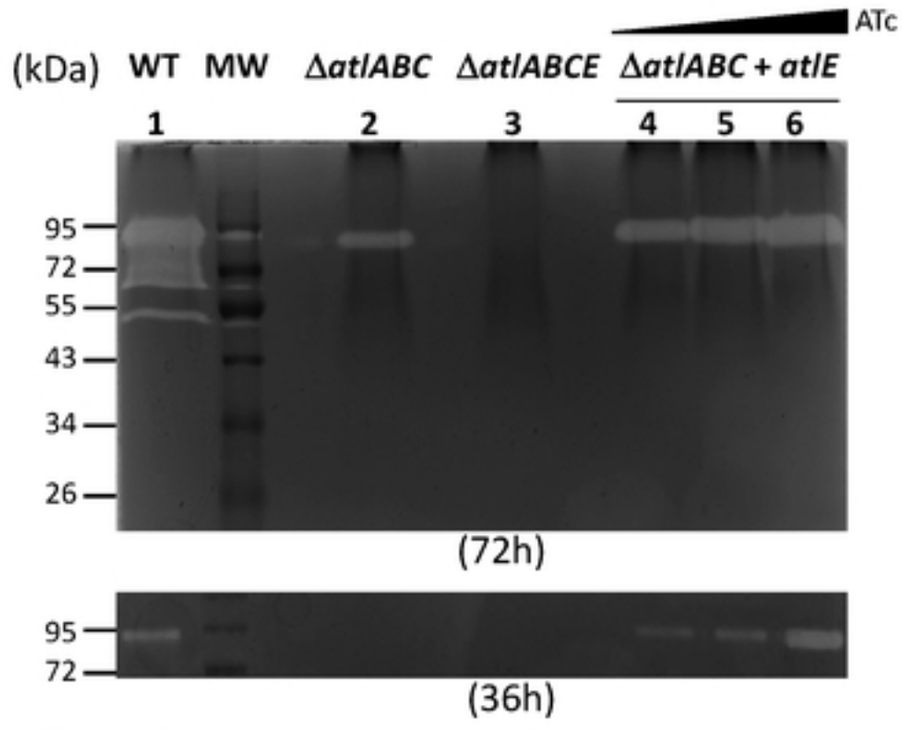

Fig. 2. Zymogram analysis of *E. faecalis* culture supernatants. Peptidoglycan hydrolytic activities were detected in 20 µL of culture supernatants of strains JH2-2 (WT, lane 1), Δ*atlABC* (lane 2), Δ*atlABCE* (lane 3) and Δ*atlABC* + *atlE* (complemented Δ*atlABC* mutant, lanes 4-6). Cells from the triple class A PBP mutant Δ*ponA* Δ*pbpF* Δ*pbpZ* were used as a substrate. The expression of *atlE* was detected in the absence (lane 4) or presence of anhydrotetracycline (Atc) at a concentration of 10 ng/µL (lane 5) or 200 ng/µL (lane 6). The zymogram was repeated with a renaturation time of 36h instead of 72h to see the increased amount of activity associated with *atlE* induction.

Figure 2 (Zymogram analysis of mutants)

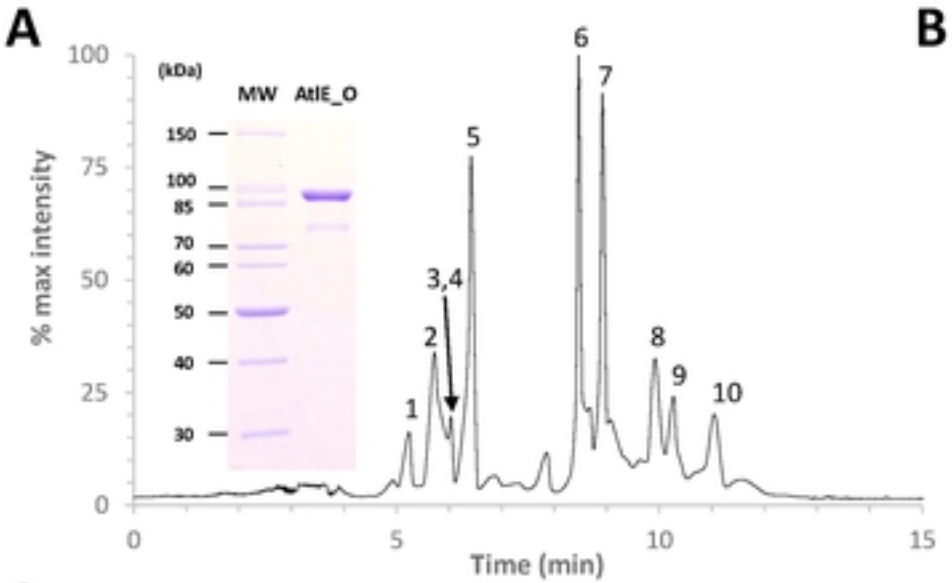

B

Peak	Inferred structure [a]	Monoisotopic mass (Da) [b]		Δppm
		Obs	Theo	
1	gm-AQKA	896.4318	896.4339	-2.3
2	gm-AQK[AA]	967.4704	967.4710	-0.6
3	gm-AQK[AA]A	1038.5080	1038.5081	-0.1
4	gm-AQK[AA]AG	1095.5298	1095.5300	-0.2
5	gm-AQK[AA]AA	1109.5443	1109.5452	-0.8
6	gm-AQK[AA]A=gm-AQK[AA]	1987.9719	1987.9685	1.7
7	gm-AQK[AA]A=gm-AQK[AA]AA	2130.0431	2130.0427	0.2
8	$(gm\text{-}AQK[AA]A)_2$=gm-AQK[AA]	3008.4699	3008.4660	1.3
9	$(gm\text{-}AQK[AA]A)_2$=gm-AQK[AA]AA	3150.5018	3150.5402	-12.2
10	$(gm\text{-}AQK[AA]A)_3$=gm-AQK[AA]AA	4171.0208	4171.0377	-4.1

[a] g, GlcNAc; m, reduced MurNAc; residues in the lateral chain are in square brackets.
[b] Obs, observed; Theo, theoretical.

C

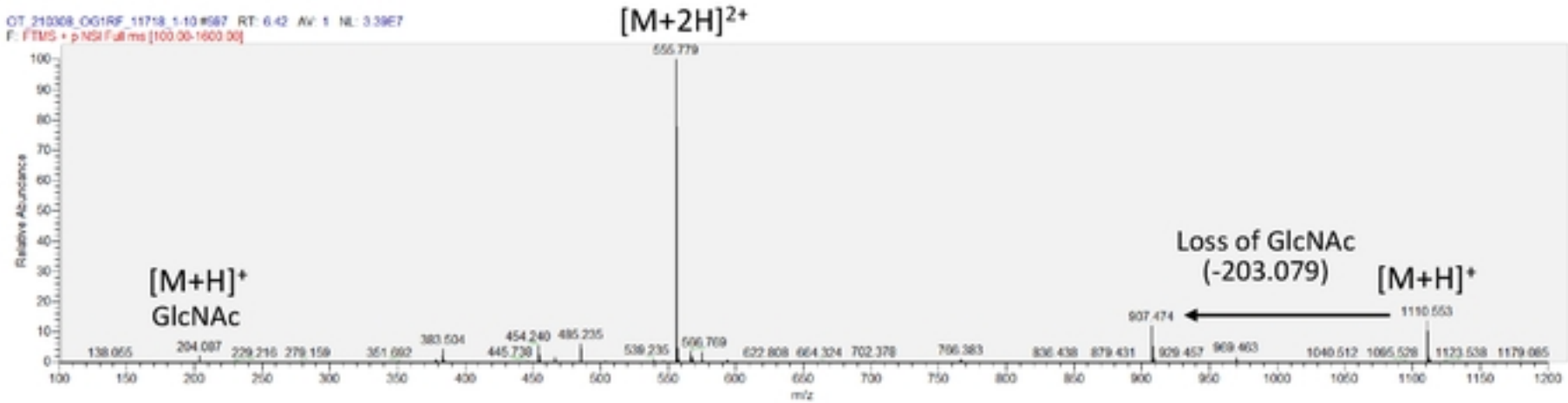

Fig. 5. LC-MS characterisation of AtlE enzymatic activity. **A**, Total Ion Count chromatgram corresponding to the OG1RF muropeptide solubilised by AtlE_O. Major peaks are numbered. The inserts shows and SDS-PAGE of AtlE_O purified by immobilised meta affinity chromatography. **B**, Identification of major muropeptides shown in A. **C**, Extracted ion chromatogram corresponding to the major monomer (peak 5), showing singly and doubly charged ions matching the expected m/z value for a disaccharide heptapeptide containing a pentapeptide stem and two L-Anine reside in the lateral chain. The loss of a non-reduced GlcNAc residue shows the N-acetylmuramidase activity of the enzyme.

Figure 5 (LC-MS analysis of AtlE activity)

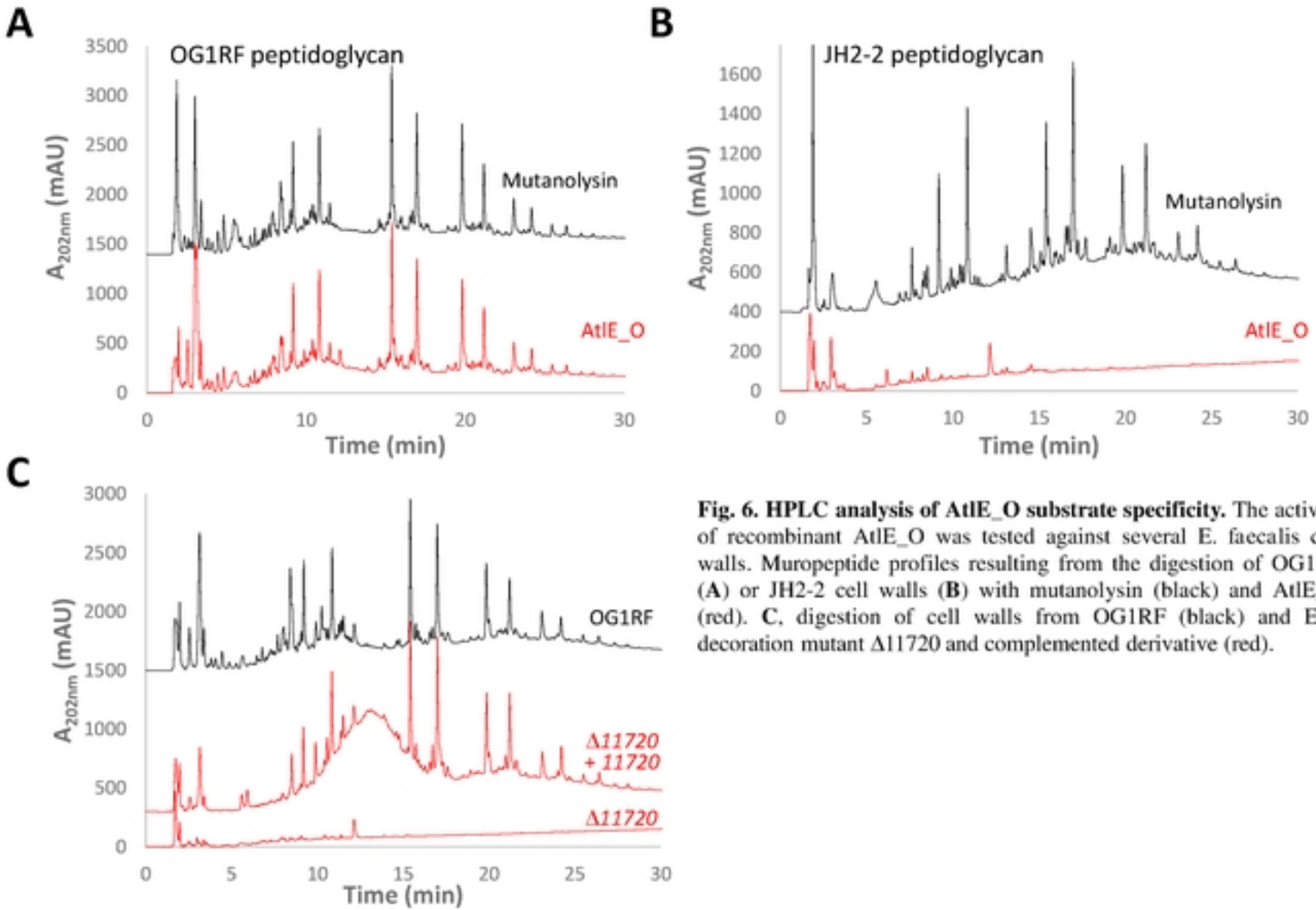

Fig. 6. HPLC analysis of AtlE_O substrate specificity. The activity of recombinant AtlE_O was tested against several E. faecalis cell walls. Muropeptide profiles resulting from the digestion of OG1RF (**A**) or JH2-2 cell walls (**B**) with mutanolysin (black) and AtlE_O (red). **C**, digestion of cell walls from OG1RF (black) and EPA decoration mutant Δ11720 and complemented derivative (red).

Figure 6 (HPLC analysis of cell wall digestion)

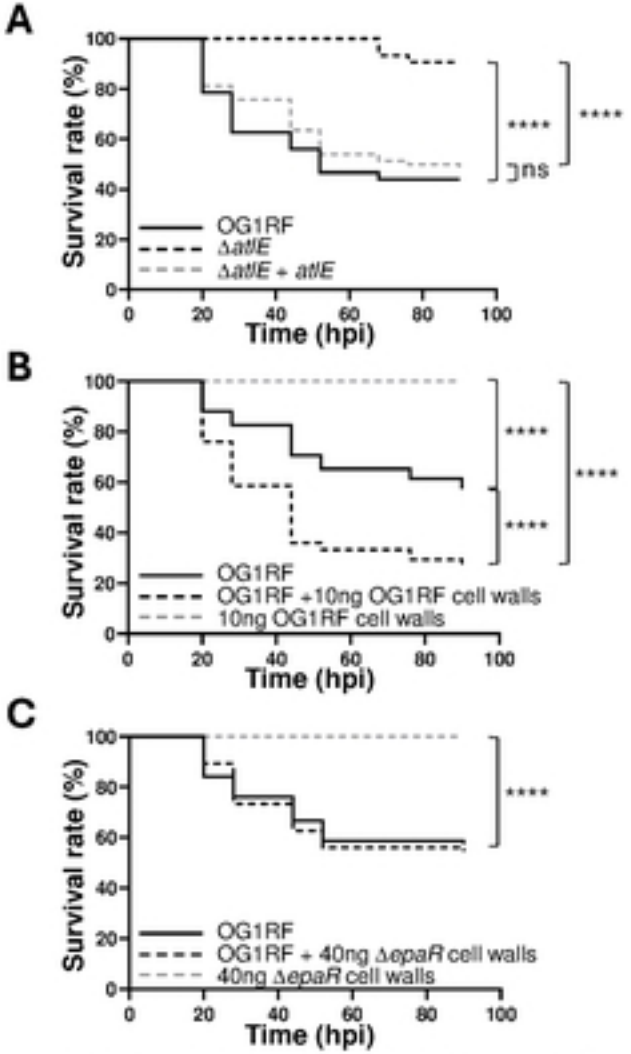

Fig. 7. Contribution of AtlE activity to E. faecalis virulence. A, Survival of zebrafish larvae following injection with c.a. 2,000 CFUs of strains OG1RF, ΔatlE and complemented derivative (ΔatlE +atlE). **B**, Injection of OG1RF in the presence of 10 ng of OG1RF soluble cell wall fragments. **C**, Injection of OG1RF in the presence of 40 ng of ΔepaR soluble cell wall fragments. Each panel combines three independent experiments (individual repeats are shown in Fig. S5-S7); each survival curve corresponds to the injection of 25 embryos. ****, P<0.0001.

Figure 7 (zebrrafish)

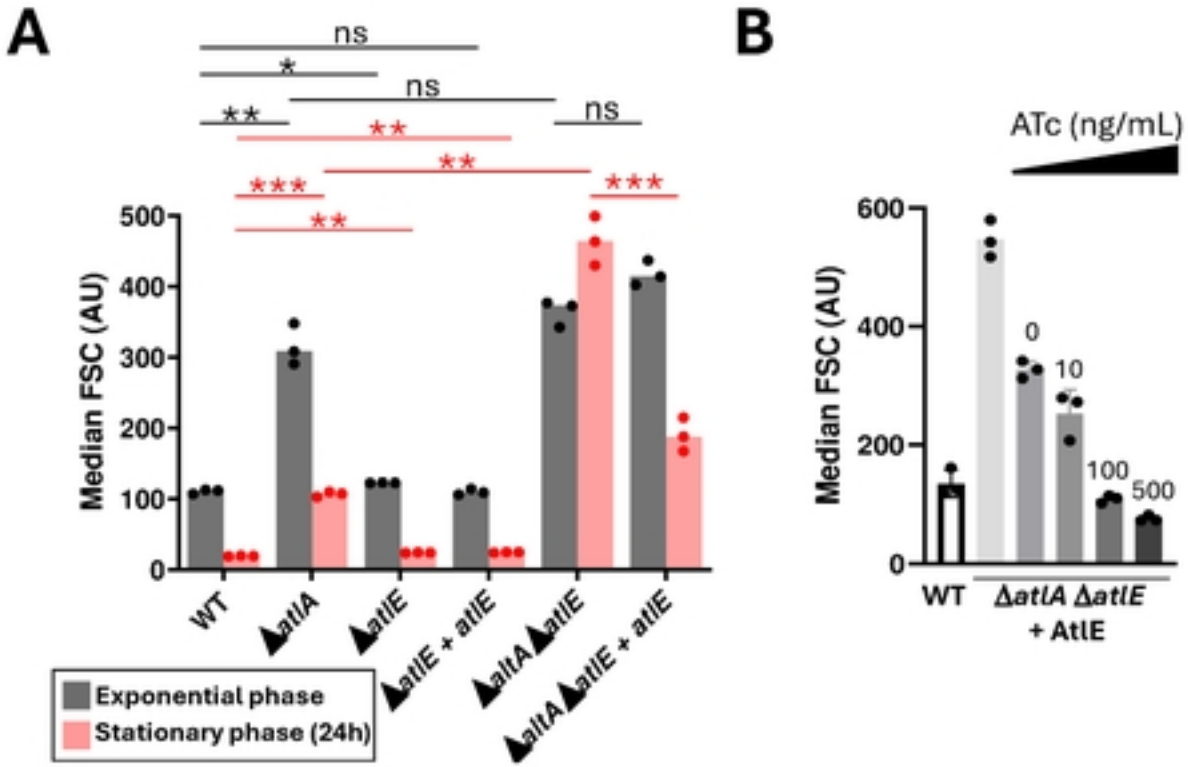

Fig. 3. Contribution of AtlE to septum cleavage and bacterial cell chain lenght. A. Comparison of median forward scattered (FSC) light values corresponding to the cell chain lengths of OG1RF (WT), ΔatlA, ΔatlE, ΔatlE + atlE (complemented deletion strain), ΔatlA ΔatlE and ΔatlA ΔatlE + atlE strains in exponentially growing cells and after 24h of growth. Statistical analyses were carried out on results from biological triplicates using t-tests with Welch's correction. For exponential cells (grey bars): WT versus ΔatlA, **, P=0.0067; WT versus ΔatlE, *, P=0.0164; WT versus ΔatlE + atlE, ns, P=0.7309; ΔatlA versus ΔatlE, ns, P=0.1025; ΔatlA ΔatlE versus ΔatlA ΔatlE + atlE, ns, P=0.1249. For stationary cells (24h cultures, pink bars): WT versus ΔatlA, ***, P=0.0005; WT versus ΔatlE, **, P=0.0064; WT versus ΔatlE + atlE, **, P=0.0012; ΔatlA versus ΔatlA ΔatlE , **, P=0.0036; ΔatlA ΔatlE versus ΔatlA ΔatlE + atlE, ***, P=0.0005. **B.** AtlE-mediated cleavage of bacterial septum. Median forward scattered (FSC) of WT, ΔatlA ΔatlE mutant and complemented ΔatlA ΔatlE + atlE derivative cells was measured after 16h of growth (overnight cultures). Anhydrotetracycline (Atc) was added at various concentration (0, 10, 200 and 500 ng/mL) to induce the expression of atlE.

Figure 3 (Flow cytometry)

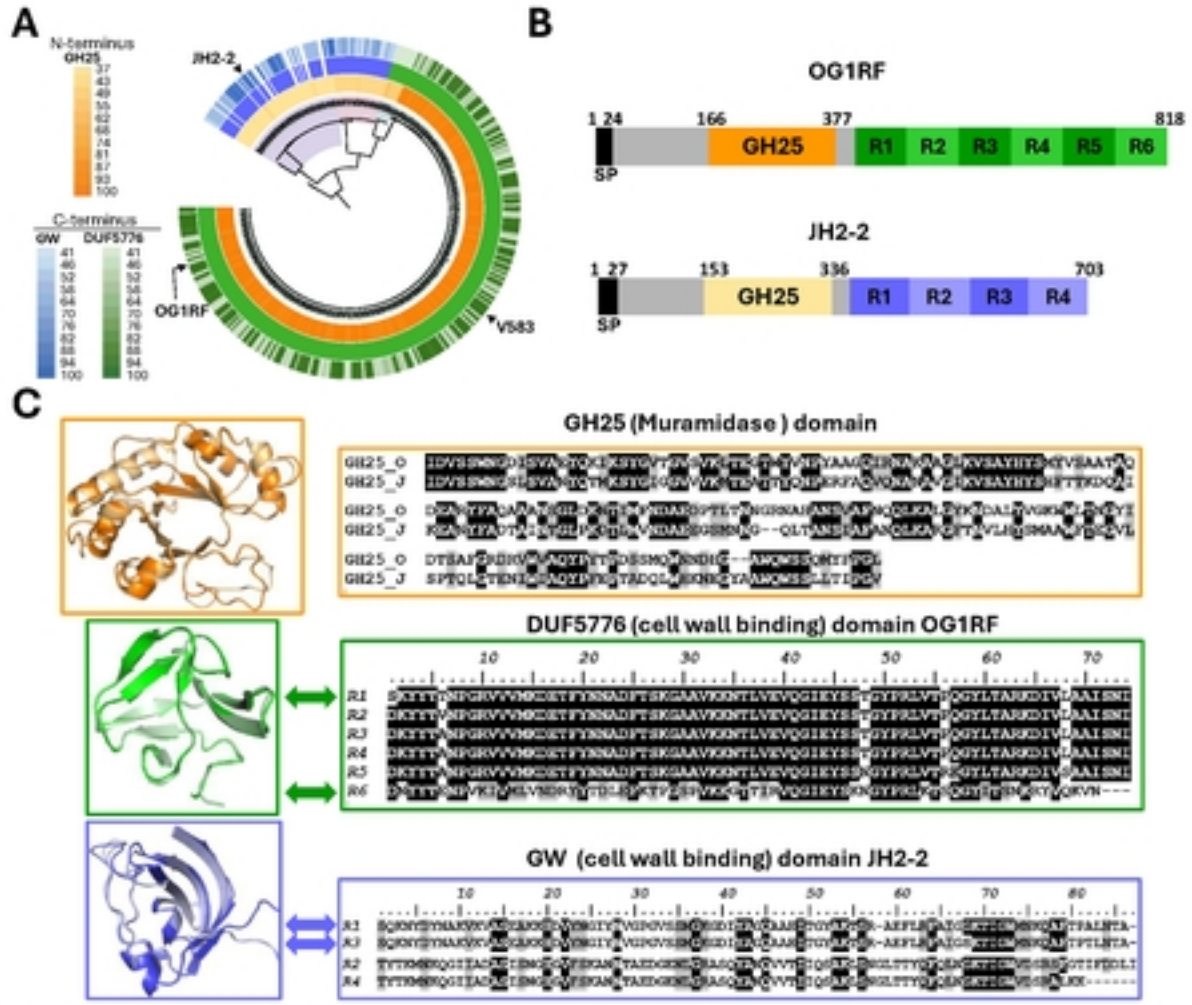

Fig. 4. Distribution and allelic variation of the E. faecalis atlE gene. A, Phylogenetic reconstruction of AtlE identified in E. faecalis genomes. Open reading frames were trimmed to contain only the GH25 domain, totalling 196 sites of which 167 were parsimony informative. Evolutionary distance was inferred using the Maximum Likelihood method using the WAG+G4 best fit model. E. faecalis V583 GH25 (N-terminus, inner ring) and DUF5776 (C-terminus, outer ring, green) domains and E. faecalis JH2-2 GW (C-terminus, outer ring, blue) domains were used as references for sequence comparisons. **B**, Domain organisation of OG1RF and JH2-2 AtlE alleles. Residues numbers are indicated on the top of the sequence; Individual DUF5776 and GW repeats are numbered from N to C-terminus. SP, signal peptide. **C**, Alphafold structure predictions of GH25, DUF5776 and GW domains from OG1RF and JH2-2. The predicted structures of two DUF5776 and GW domains showing the less similar sequences were aligned (R1 and R6 for OG1RF, R1 and R3 for JH2-2).

Figure 4 (AtlE allelic variation)